Sveučilište u Zagrebu

FAKULTET ELEKTROTEHNIKE I RAČUNARSTVA

Pavle Prentašić

RAČUNALNA ANALIZA SLIKA OČNE POZADINE ZA RANU DETEKCIJU DIJABETIČKE RETINOPATIJE

DOKTORSKI RAD

Zagreb, 2018.

Sveučilište u Zagrebu
FAKULTET ELEKTROTEHNIKE I RAČUNARSTVA

Pavle Prentašić

RAČUNALNA ANALIZA SLIKA OČNE POZADINE ZA RANU DETEKCIJU DIJABETIČKE RETINOPATIJE

DOKTORSKI RAD

Mentor: Prof. dr. sc. Sven Lončarić
Prof. dr. sc. Zoran Vatavuk

Zagreb, 2018.

University of Zagreb

FACULTY OF ELECTRICAL ENGINEERING AND COMPUTING

Pavle Prentašić

COMPUTATIONAL ANALYSIS OF FUNDUS PHOTOGRAPHS FOR EARLY DETECTION OF DIABETIC RETINOPATHY

DOCTORAL THESIS

Supervisor: Professor Sven Lončarić, PhD
Professor Zoran Vatavuk, PhD

Zagreb, 2018.

Doktorski rad izrađen je na Sveučilištu u Zagrebu Fakultetu elektrotehnike i računarstva, na Zavodu za elektroničke sustave i obradbu informacija

Mentor: prof. dr. sc. Sven Lončarić
Mentor: prof. dr. sc. Zoran Vatavuk

Doktorski rad ima: XYZ stranica

Doktorski rad br.: _____

About the Supervisor

Dr. Sven Lončarić is a full professor of electrical engineering and computer science with permanent tenure at Faculty of Electrical Engineering and Computing, University of Zagreb, Croatia. He received Diploma of Engineering and Master of Science degrees in electrical engineering from University of Zagreb Faculty of Electrical Engineering and Computing (FER) in 1985 and 1989, respectively. As a Fulbright scholar he received Doctor of Philosophy (Ph.D.) degree in electrical engineering from University of Cincinnati, USA in 1994. From 2001-2003, he was an assistant professor at New Jersey Institute of Technology, USA. His areas of research interest are digital image processing and computer vision. He was principal investigator on a number of research and development projects in image processing and analysis including applications in medicine, automotive industry, and visual quality inspection. With his students and collaborators he co-authored more than 200 publications in scientific journals and conferences. He is among the top ten cited scientists in the area of technical sciences in Croatia. He was Chair of the Department of Electronic Systems and Information Processing. He is the founder and director of the Center for Computer Vision at University of Zagreb. Prof. Lončarić is the head of the Image Processing Group. He is the Chair of the committee for development of biomedical engineering at the University of Zagreb. He is a co-director of the national Center of research excellence in data science and cooperative systems. Prof. Lončarić was the Chair of the IEEE Croatia Section. He is a senior member of IEEE and a member of Croatian Academy of Technical Sciences. Prof. Lončarić received several awards for his scientific and professional work.

O mentoru

Dr. sc. Sven Lončarić redoviti je profesor u trajnom zvanju na Fakultetu elektrotehnike i računarstva (FER) Sveučilišta u Zagrebu. Diplomirao je 1985. godine i magistrirao 1989. godine na FER-u. Kao dobitnik Fulbrajtove stipendije 1990. godine započeo je doktorski studij na Sveučilištu u Cincinnatiju, SAD, gdje je doktorirao 1994. godine u području digitalne obrade slike. Od 2001.-2003. godine bio je profesor na Sveučilištu New Jersey Institute of Technology u Newarku, SAD. Područje njegovog istraživačkog interesa su digitalna obrada slika i računalni vid. Bio je voditelj više istraživačkih i razvojnih projekata u području obrade i analize slika uključujući primjene u medicini, automobilskoj industriji i vizualnoj inspekciji kvalitete u proizvodnji. Sa svojim doktorandima i suradnicima objavio je više od 200 znanstvenih i stručnih radova u međunarodnim časopisima i na skupovima. Među deset je najviše citiranih znanstvenika u području tehničkih znanosti u Hrvatskoj. Bio je predstojnik Zavoda za elektroničke sustave i obradbu informacija FER-a. Osnivač je i voditelj Centra izvrsnosti za računalni vid na

Sveučilištu u Zagrebu. Voditelj je istraživačkog laboratorija za obradu slike na FER-u. Predsjednik je Odbora za razvoj biomedicinskog inženjerstva na Sveučilištu u Zagrebu. Suvoditelj je nacionalnog Znanstvenog centra izvrsnosti za znanost o podatcima i kooperativne sustave. Stariji je član IEEE i redoviti član Akademije tehničkih znanosti Hrvatske. Prof. Lončarić je dobitnik više nagrada za znanstveni i stručni rad.

About the Supervisor

Zoran Vatavuk finished Medical school from University in Zagreb in 1987. He finished his medical internship in 1988 at Community Health Centre in Drniš. He received Doctor of Philosophy (Ph.D.) degree in Biomedicine and Health sciences from University of Zagreb in 2004. He became associate professor in Ophthalmology in 2007 and professor in Ophthalmology in 2013. Professor Vatavuk has worked at the University department of Ophthalmology from 1996 until present day. His areas of interest are vitreoretinal disease and surgery. In 1998 he introduced vitreoretinal surgery, which was previously not performed at present Department. In 2001 he introduced photodynamic therapy in Croatia, and in 2005 intravitreal application of Avastin for the treatment of age-related macular degeneration and pathologic myopia. Professor Vatavuk has actively participated in numerous foreign and domestic ophthalmologic congresses and meetings. He has authored and co-authored numerous articles, the most of which were published in journals indexed in Current Contents. He is also author of one book chapter, as well as numerous congress abstracts. He is a reviewer for several international ophthalmology journals and serves on the editorial boards of several scientific journals. He has been the head of the Croatian Ophthalmological Society since 2008.

O mentoru

Zoran Vatavuk je završio Medicinski fakultet na Sveučilištu u Zagrebu 1987. godine. Nakon toga je odradio medinski staž u domu zdravlja Drniš. Doktorirao je biomedicinu i zdravstvene znanosti 2004. godine na Sveučilištu u Zagrebu. Postao je izvanredni profesor 2007. godine te profesor 2013. godine. Profesor Vatavuk radi na sveučilišnom odjelu oftalmološke klinike od 1996. godine KBC Sestre Milosrdnice. Njegovo područje intersea uključuje vitreoretinalne bolesti i operacije oka. 1998. godine uveo je vitreoretinalne operacije u vrijeme kada se takve operacije nisu provodile na odjelu za oftalmologiju. U 2001. godini uveo je fotodinamičke terapije oka u Republiku Hrvatsku kao i intravitrealnu primjenu Avastina za liječenje makularne degeneracije i patološke mijopije. Profesor Vatavuk je aktivno sudjelovao na mnogobrojnim međunarodnim kao i domaćim oftalmološkim kongresima i sastancima. Autor je te koautor brojnih znanstvenih članaka od kojih je većina indeksirana u Current Contents sustavu indeksacije. Autor je jednog poglavlja knjige kao i autor mnogbrojnih sažetaka znanstvenih skupova. Profesor Vatavuk je recenzent velikog broja međunarodnih časopisa iz područja oftalmologije te urednik nekolicine znanstvenih časopisa. Predsjednik je Hrvatskog oftalmološkog društva od 2008. godine.

Sažetak

Dijabetička retinopatija je jedna od glavnih kroničnih bolesti i jedan od glavnih uzroka sljepoće koja se može spriječiti u svijetu. Kako bi se postigla rana dijagnoza puno truda se mora uložiti u sustave automatskog probira pacijenata temeljene na slikama očne pozadine. Ova doktorska disertacija se bavi istraživanjem naprednih metoda obrade i analize slika koje su potrebne za razvoj automatskih sustava probira pacijenata. Prvi znanstveni doprinos je baza od pedeset slika očne pozadine koja sadrži slike zdravih, ali i osoba koje imaju dijabetičku retinopatiju. Baza slika sadrži i oznake normalnih kao i patoloških struktura. Slike su označila pet oftalmologa te se baza koristi za razvoj i validaciju algoritama. Drugi znanstveni doprinos je metoda za detekciju krvnih žila u slikama očne pozadine temeljena na modeliranju i višerazinskom praćenju krvnih žila. Kako bismo locirali optički disk koji se nalazi u svakoj slici očne pozadine razvijena je metoda za lociranje optičkog diska temeljena na glasanju i stohastičkom učenju te ta metoda predstaclja treći važni doprinos ove disertacije. Unutar disertacije pokazujemo kako ovaj pristup daje bolje rezultate od individualnih algoritama koji su dio ansambla algoritama. Kako bismo detektirali eksudate koji su jedan od najvažnijih prvih simptoma prilikom dijagnoze dijabetičke retinopatije razvijena je metoda koja kombinira izlaz duboke konvolucijske neuronske mreže sa specifičnim oftalmološkim znanjem unutar ekspertnog sustava. Ta metoda predstavlja četvrti znanstveni doprinos disertacije. Na kraju disertacije dajemo pregled rada te se daju prijedlozi za poboljšanje performansi sustava.

Ključne riječi: Dijabetička retinopatija, slike očne pozadine, obrada i analiza slike, strojno učenje, neuronske mreže, duboko učenje

Abstract

Diabetic retinopathy is one of the leading disabling chronic diseases, and one of the leading causes of preventable blindness in the world. In order to achieve early diagnosis of diabetic retinopathy a major effort will have to be invested into automatic screening systems using color fundus photographs. This thesis investigates advanced image processing and analysis methods, which are needed for automatic screening system development. The first contribution of this thesis work is a database of fifty fundus images from healthy and diabetic patients. The database has normal and pathological structures labeled by five ophthalmology experts and is used for algorithm development and testing. The second contribution is a method for blood vessel segmentation from fundus photographs using model-based multi-scale vessel tracking. In order to locate the optic disc, which is present in all fundus photographs, a method based on a voting-based classifier and stochastic learning is presented as one of the thesis contributions. We show

that this approach easily outperforms methods which are part of the classifier ensemble. In order to detect exudates, which are one of the most important early signs of diabetic retinopathy, a method based on combining a deep convolutional neural network with specific ophthalmic knowledge in one expert system was developed and represents the last thesis contribution. In the end, the thesis gives a summary of the work with considerations about potential performance improvements.

Keywords: diabetic retinopathy, funds photographs, image processing and analysis, machine learning, neural networks, deep learning

Prošireni sažetak

Dijabetička retinopatija je jedna od glavnih kroničnih bolesti i jedan od glavnih uzroka sljepoće koja se može spriječiti u svijetu. Rana dijagnoza dijabetičke retinopatije je bitna jer se smanjuje teret bolesti na pacijenta i obitelji obzirom da se ranom detekcijom može zadržati dovoljna kvaliteta vida pogođene osobe što na kraju ipak vodi do bolje kvalitete života. Kako bi se postigla rana dijagnoza moraju se razviti sustavi za automatsku ranu dijagnozu temeljeni na slikama očne pozadine. Slike očne pozadine su korisne za utvrđivanje stadija dijabetičke retinopatije obzirom da je krvožilni sustav oka izrazito osjetljiv na promjene izazvane dijabetičkom retinopatijom te zbog svog neinvazivnog karaktera. Naglasak ove doktorske disertacije je na istraživanju naprednih metoda obrade i analize slika koje su potrebne za razvoj automatskih sustava probira pacijenata. Kako bi se razvio sustav automatskog probira pacijenata za dijabetičku retinopatiju potrebno je razviti metode za segmentaciju normalnih struktura kao što su krvne žile, optički disk te žuta pjega te segmentaciju patoloških struktura koje su prisutne samo u slikama očne pozadine pacijenata oboljelih od dijabetičke retinopatije kao što su tvrdi i meki eksudati, točkasta te mrljata krvarenja i neovaskularizacije.

Prilikom istraživanja prvi korak je bio prikupljanje baze slika koja se kasnije koristila za razvoj te testiranje metoda obrade i analize slika. Baza slika se sastoji od 50 slika pri čemu su u bazi prisutne slike zdravih te osoba oboljelih od dijabetičke retinopatije. Slike sadrže označene normalne strukture kao što su optički disk, makula te krvne žile kao i patološke strukture poput eksudata, krvarenja i neovaskularizacija. Svaku sliku je označilo pet stručnjaka oftalmologa.

Nakon prikupljanja baze slika razvijena je metoda za detekciju optičkog diska koji je pristuan u svim slikama očne pozadine. Metoda se temelji na kombiniraju izlaza više jednostavnih metoda kako bi se postigla bolja točnost detekcije. Težine pojedine metode su određene algoritmom simuliranog kaljenja. U disertaciji se pokazuje da je točnost ove metode značajno veća u odnosu na pojedine metode koje čine ansambl. Osim metode za detekciju optičkog diska razvijena je metoda za detekciju krvnih žila kao još jedne od struktura koje su prisutne u svim slikama. Metoda se temelji na višerazinskom praćenju i modeliranju krvnih žila. Obzirom na činjenicu da krvne žile imaju specifičan profil korišten je model krvnih žila čiji parametri su dinamički mijenjani optimizacijskom procedurom. Osim toga, modeliranje krvnih žila se nije primjenjivalo direktno na slikama već na slikama u kojem su metodom filtriranja krvne žile bile pojačane.

Nakon toga razvijene su metode za detekciju eksudata. U disertaciji su objašnjenje dvije metode. Prva metoda se temelji na postupku koji je sličan postupku detekcije optičkog diska gdje se kombiniraju jednostavnije metode kako bi se povećala točnost detekcije. Drugi pristup se temelji na razvoju ekspertnog sustava unutar kojeg se kombinira izlaz duboke konvolucijske neuronske mreže sa specifičnim oftalmološkim znanjem koje povećava ukupnu točnost seg-

mentacije eksudata. Kako bi se iskoristilo specifično oftalmološko znanje potrebno je iskoristiti izlaze detektora krvnih žila te optičkog diska sa izlazom duboke neuronske mreže. Kombiniranjem izlaza stvorena je mapa vjerojatnosti prisutnosti eksudata na određenoj lokaciji. Postavljanjem praga mogu se dobiti potencijalna područja eksudata. Nakon izlučivanja potencijalnih regija računaju se značajki za svako područje te se na kraju korištenjem klasifikatora donosi odluka je li riječ o eksudatu ili ne. Unutar disertacije pokazuju se rezultati koji govori da je riječ o dosta robusnom rješenju za detekciju eksudata.

Na kraju disertacije daje se kratak pregled ostvarenih rezultata te se daju smjernice o potencijalnim poboljšanjima razvijenih metoda.

Ključne riječi: Dijabetička retinopatija,slike očne pozadine, obrada i analiza slike, strojno učenje, neuronske mreže, duboko učenje

Sadržaj

1. Introduction 1

2. Overview of existing methods 5

2.1. Detection of blood vessels 5

2.2. Detection of microaneurysms and hemorrhages 7

2.3. Detection of exudates 9

2.4. Detection of neovascularizations 11

3. Framework for validation of retinal segmentation methods 12

3.1. Overview of existing databases 12

3.1.1. DRIVE database 12

3.1.2. STARE database 13

3.1.3. ARIA online 13

3.1.4. ImageRet 13

3.1.5. Messidor 14

3.1.6. Review 14

3.1.7. ROC microaneurysm set 14

3.1.8. VICAVR 15

3.2. Dibetic retinopathy image database (DRiDB) 15

4. Optic disc detection using a voting based classifier and stochastic learning 20

4.1. Individual optic disc detection algorithms 21

4.1.1. Hough transformation of vessels approach 22

4.1.2. Pyramidal decomposition approach 22

4.1.3. Vessel direction matched filtering (VDM) approach 22

4.1.4. Fuzzy convergence approach 23

4.1.5. Brightness approach 24

4.1.6. LoG filtering approach 24

4.1.7. Entropy approach 24

4.2. Combining different probability maps 25

4.3. Performance evaluation 27

5. Blood vessel segmentation from fundus photographs using model-based multi-scale vessel tracking 28
5.1. One-dimensional blood vessel models 30
5.2. Two-dimensional blood vessel model 31
5.3. Blood vessel enhancement 32
5.4. Blood vessel tracking 35
5.5. Seed point generation 37
5.6. Performance evaluation 37

6. Exudate detection using voting-based classifier and stochastic learning 40
6.1. Weighted ensemble based exudate detection 42
6.1.1. Preprocessing methods 42
6.1.2. Candidate extraction algorithms 44
6.1.3. Combining candidate extraction algorithms 46
6.1.4. Exudate classification 47
6.2. Performance evaluation 48

7. Automatic early detection of diabetic retinopathy using rule-based system and specific ophthalmologic knowledge 51
7.1. Detection of bright borders 53
7.2. Parabola fitting 55
7.3. Convolutional neural network for exudate detection 57
7.3.1. Preprocessing 57
7.3.2. Convolutional neural network architecture 59
7.4. Performance evaluation 61

8. Conclusion 63

Literatura 65

Životopis 76

Biography 77

Chapter 1

Introduction

Diabetes is a well known disease and may cause abnormalities in the retina (diabetic retinopathy), kidneys (diabetic nephropathy), nervous system (diabetic neuropathy) and is known to be a major risk for cardiovascular diseases. Diabetic retinopathy (DR) is a microvascular complication caused by diabetes which can lead to blindness. In early stages of diabetic retinopathy typically there are no visible signs but the number and severity of abnormalities increase during the time. Diabetic retinopathy typically starts with small changes in retinal capillaries. The first detectable abnormalities are microaneurysms which represent local enlargements of the retinal capillaries. The ruptured microaneurysms can cause hemorrhages. After a period of time, hard exudates may appear. The hard exudates are lipid formations leaking from weakened blood vessels. As the retinopathy advances, the blood vessels may become obstructed which causes microinfarcts in the retina. These microinfarcts are called soft exudates. Extensive lack of oxygen caused by microinfarcts causes the development of new fragile vessels. This phenomenon is called neovascularization which is a serious eyesight threatening state and may cause sudden loss in visual acuity or even permanent blindness. Examples of microaneurysms, hemorrhages, hard exudates, soft exudates and neovascularization are visible in Fig. 1.1.

Diabetic retinopathy is one of the leading disabling chronic diseases, and one of the leading causes of preventable blindness in the world [1]. It was found to be the fourth most frequently managed chronic disease in general practice in 2009, and the projections go as high as the second most frequent disease by the year 2030 [1]. The global burden of diabetic patients is expected to rise from 171 million in 2000 to 366 million in 2030 [1]. In Europe more than 52.8 million people are diagnosed with diabetes with the number expected to rise to 64 million by 2030. In Croatia about 300 thousand people are estimated to have diabetes and of those only 190 thousand are registered, which complicates the treatment. Early diagnosis of diabetic retinopathy enables timely treatment that can ease the burden of the disease on the patients and their families by maintaining a sufficient quality of vision and preventing severe vision loss and blindness [2]. In addition to the obvious medical benefits, significant positive economical

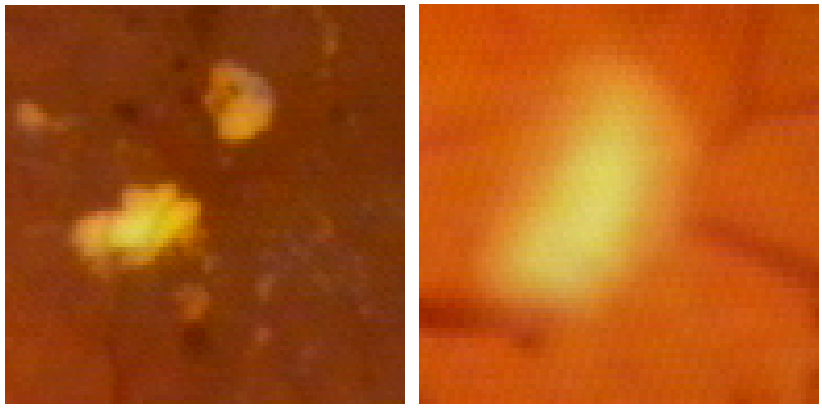

(a) Hard exudates (b) Soft exudate

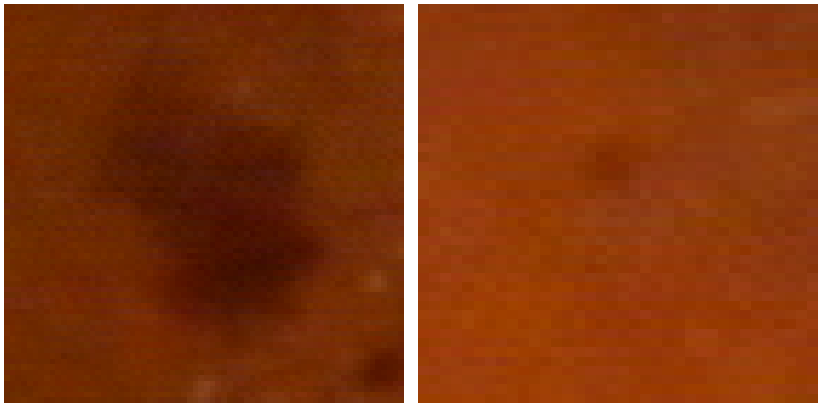

(c) Hemorrhages (d) Microaneurysm

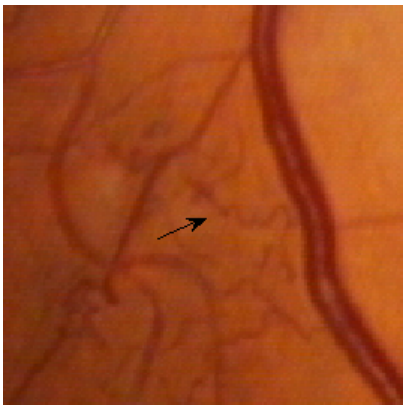

(e) Neovascularizations

Fig. 1.1: Abnormal findings in the eye fundus images caused by diabetic retinopathy

effects are achieved by maintaining patient's workability and self-sustainability.

In order to achieve early diagnosis of diabetic retinopathy a major effort will have to be invested into screening programs. Screening is important as up to one third of people with diabetes may have progressive DR changes without symptoms of reduced vision [3], thus allowing the disease to progress and making treatment difficult. Systematic screening programs for diabetic eye disease have been developed in many countries [4, 5, 6]. In the UK, the NHS Diabetic Screening Program offers annual fundus photography for all patients with diabetes

over the age of 12, regardless of their socio-economic status [6].

In current screening programs only color fundus photography is used, and the data is sent to a grading center for reading where expert human readers estimate the disease severity. The main disadvantage is the necessity for qualified experts to grade the images, e.g. in the NHS Diabetes Screening Program one patient's images can be graded by up to four different experts. This standard is impossible to achieve in countries with a shortage of qualified medical personnel and due to high costs of such a labor intensive medical procedure.

Fundus imaging has an important role in diabetic retinopathy detection and monitoring because eye fundus is sensitive to vascular diseases and we can consider fundus imaging as a candidate for non-invasive screening. The success of this type of screening approach depends on accurate fundus image capturing, and especially, on accurate and robust image processing and analysis algorithms for abnormalities detection.

The aim of this doctoral research was the development of methods for automated early detection of diabetic retinopathy from color fundus photographs. The developed methods could be used in regular screening programs of patients with diabetes, which would reduce the health issues caused by diabetic retinopathy. In order to develop a system for automated early detection of diabetic reitnopathy methods for detection of normal and pathological structures were researched and developed. The approach applied in this research is based on advanced image processing and analysis methods, which includes application of machine learning techniques.

The main contributions of this thesis are as follows:

- Method for blood vessel segmentation from fundus photographs using model-based multi-scale vessel tracking
- Method for segmentation of normal and pathological retinal structures using voting-based classifier and stochastic learning
- Method for automatic early detection of diabetic retinopathy using rule-based expert system and specific ophthalmologic knowledge about normal and pathological retinal anatomy
- Image database for testing of segmentation methods of normal and pathological retinal structures, which contains segmentations of normal and pathological structures from multiple experts

The dissertation starts with a short overview of existing methods for automatic early detection of diabetic retinopathy. In Chapter 3 the image database for testing of segmentation methods of normal and pathological structures is explained in more detail. In Chapter 5 details of a method for blood vessel segmentation using model-based multi-scale vessel tracking in fundus photographs is explained in more detail. In Chapter 4 a newly developed method for segmentation of the optical disc using a voting based classifier and stochastic learning is explained. A method for segmentation of exudates, which represent one of the key pathological structures in

images from patients with diabetic retinopathy, based on a voting based classifier with stochastic learning, is explained in Chapter 6. In order to improve the overall performance of a system for early detection of diabetic retinopathy results of normal and pathological structure detection outputs can be combined using a rule based expert system and specific knowledge about the normal and pathological anatomy. Details of a methods which incorporates specific ophthalmic knowledge is presented in Chapter 7. In Chapter 8 a short conclusion is given with an overview of potential performance improvements to currently developed methods and systems for early detection of diabetic retinopathy.

Chapter 2

Overview of existing methods

In literature, different methods and approaches for automatic early detection of diabetic retinopathy can be found. Because diabetic retinopathy can be characterized by different pathological changes visible in fundus photographs different image processing and analysis methods can be used to detect such structures. In this chapter we give a short overview of exisiting methods for detection of normal and pathological structures.

2.1 Detection of blood vessels

Blood vessels appear as dark curvilinear structures and present a useful reference for pathological structures, which are present in images belonging to patients with diabetic retinopathy. In the literature different methods for blood vessel detection exist. A nice overview of different approaches can be found in [7]. We can find methods based on pattern recognition techniques, matched filtering, vessel tracking, mathematical morphology, mutiscale filtering based approaches and model based approaches. Pattern recognition techniques can be divided into supervised and unsupervised approaches.

For example, in [8] authors represented each pixel by a feature vector composed of the pixel's intensity and two-dimensional Gabor wavelet transform responses taken at multiple scales. A Bayesian classifier in which each class-conditional probability density function is described as a linear combination of Gaussian functions is used to classify each pixel as either a vessel or non-vessel pixel.

In [9] authors presented an unsupervised fuzzy based vessel segmentation approach. Intensity information from red and green channels is first used to correct non-uniform illumination and matched filtering is used to enhance the blood vessel contrast with regards to the background. In order to classify the pixels, a spatially weighted fuzzy C-means clustering followed by connected component labeling is used.

In [10] a method which uses match filtering and Ant colony optimization algorithm for blood

vessel segmentation is presented. The image is first preprocessed and then a match filtering approach is used to enhance the blood vessels. Ant colony optimization is applied in parallel to matched filtering. The results are combined followed by length filtering in order to extract the complete vasculature network.

In [11] authors presented a method, which combines morphological mutiscale enhancement with fuzzy filtering and watershed transformation. The background is first estimated using non linear multiscale morphology opening operators with a varying size of structuring element. The background estimated images is subtracted from the original image for contrast normalization. The normalized image is then processed by a combined fuzzy morphological operation with twelve linear structuring elements rotated every 15 degrees between zero and 180 degrees with nine pixels length. In order to obtain vessel regions the filtered image is thresholded followed by a thinning operation to approximate the vessel centerlines. Finally, the vessel boundaries are detected using watershed techniques with the obtained vessel centerlines.

A method using regularization based multiconcavity modeling is presented in [12]. The method is able to handle both normal and pathological retinas with bright and dark lesions simultaneously. Three different concavity measures are proposed to detect blood vessels. Each of these concavity measures is designed to address the negative impact of lesions for identifying the normal vessels. The steep intensity transition pattern of bright lesions is distinguished from vessels with differential concavity measures. A line shape concavity measure is used to distinguish the irregular shape intensity structure of dark lesions from the line shape intensity structure of the blood vessel. A locally normalized concavity measure is used to filter out the noise. Finally, the features obtained from these concavity measures are combined according to their statistical and geometrical properties and later a lifting technique is used for optimizing the regularized solution towards the ideal vessel shape.

In [13] a method based on nonlinear projections is presented. The nonlinear projection is used to capture the texture structures in image. First, the green channel of the original image is projected onto a closed convex set. The set consists of oscillating functions with zero mean. The oscillating components of scanning retinal images are adopted to capture the features of blood vessel networks. In order to obtain a segmented vessel tree an adaptive thresholding method based on the variational image binarization algorithm is applied. In order to reduce noise, morphological post processing is applied to the obtained binary image

In [14] a three-stage blood vessel segmentation algorithm for color fundus photographs is presented. In the first stage, the green channel of the fundus image is preprocessed and a binary image representing blood vessel using high pass filtering is extracted. A second binary image is created from the morphologically reconstructed enhanced image. In order to improve performance, regions common to both binary images are combined to extract major vessels. In the second stage, all remaining pixels in the two binary images are classified using a Ga-

ussian mixture model classifier using a set of eight features that are extracted based on pixel neighborhood and first and second-order gradient images. In the third, postprocessing stage, blood vessels obtained in the first stage are combined with the classified vessel pixels in order to obtain the final vessel map.

In [15] authors have devised a computational imaging framework using deep and ensemble learning for detection of blood vessels in color fundus photographs images. An ensemble of deep convolutional neural networks is trained to segment vessel and non-vessel areas of a color fundus photographs. Each convolutional neural network has three convolutional layers and two fully connected layers and is trained independently on randomly selected patches from the training images. At the time of inference, the vesselness-probabilities independently output by each convolutonal neural network are averaged to form the final vesselness probability of each pixel.

2.2 Detection of microaneurysms and hemorrhages

Detection of microaneurysms in fundus photographs is very important because this structures represent one of the earliest signs of diabetic retinopathy. In literature, different methods exist. For example, in [16] authors present a methods, which starts with blood vessel detection. After that, rotational cross-sectional profile analysis on the regional maximum pixels is performed. The statistical parameters like mean, standard deviation, coefficient of variation of feature set are calculated. The microaneurysm candidates are estimated using a Naive Bayes classifier.

In [17] authors use different preprocessing methods such as gamma correction, green channel extraction, location based contrast enhancement to improve the visibility of microaneurysms in color fundus photographs. Different features using Gray Level Co-occurrence Matrix, wavelet and first order statistics are extracted. After that, a k nearest neighbor classifier is used to remove spurious candidates. The remaining candidates are thresholded to obtain the final binary output representing microaneurysms.

In [18] authors used a multiscale Bayesian correlation filtering approach. In this approach responses from a Gaussian filterbank are used to construct probabilistic models of an object and its surroundings. A correlation measure is obtained by matching the filter outputs in a new image with a trained model. When the responses of the correlation filtering are larger than a threshold, the detected locations are regarded as candidate microaneurysms. An adaptive thresholding scheme is applied to segment the vasculature and all candidates on the vasculature are removed. Region growing is used to segment the candidate microaneurysms. After segmentation, a large set of features based on shape, grayscale and color pixel intensity, responses of Gaussian filter-banks and correlation coefficient values are extracted from each candidate. The minimum and maximum values of each feature for all true lesions are placed in a discrimination

table. This is used to remove any candidates whose features are below the minimum or greater than the maximum defined in the discrimination table. The remaining candidates after this stage are classified as true red lesions.

In [19] candidate detection is performed on the green plane of the color image. The image is first resized so that the field of view has a fixed width and the image is normalized by subtracting an estimate of the image background. The estimate is determined by median filtering using a large kernel. The candidate detection step is performed on the median filtering normalized image using an unsupervised mixture model based clustering method. It is assumed that all pixels in the image are part of one of three classes: background elements, foreground elements, such as vessels, optic disk and lesions and a third class representing outliers. A three class Gaussian mixture model is fitted to image intensities and a group of microaneurysm candidates are segmented by thresholding the fitted model. Vessel segmentation is performed to remove those detected candidates that lie on the vasculature. Using logistic regression, a likelihood for each of the remaining microaneurysm candidates is generated based on their color, shape and texture characteristics.

In [20] a method consisting of a preprocessing, candidate extraction, feature extraction and classification is proposed. Because retinal fundus images often have nonuniform illumination, poor contrast and noise images and because microaneurysms are hardly visible in regions of low brightness and poor contrast multiple preprocessing steps are performed on the inverted green channel of the input image. Authors start with illumination equalization according to (2.1).

$$I_{ie} = I - I_{bg} = u \tag{2.1}$$

Here, I_{bg} represents a background image generated by mean filtering of the original image, and u represents the average intensity of the original image I to keep the same gray level range as the original image. After illumination equalization, contrast limited adaptive histogram equalization is performed in order to increase local contrast. Finally, image smoothing is performed to reduce the noise level present in each fundus image. After preprocessing, a candidate extraction step is performed. As microaneurysms appear as bright structures in the preprocessed image, the microaneurysm region contains at least one regional maximum. Thus, the local maximum pixels can be considered as microaneurysm candidates. However, a large amount of noise will be extracted in this way. In order to overcome this limitation, peak detection is applied on each profile and a set of line detectors of different orientations are applied to each local maximum pixel to examine the surrounding, whose central pixel is the local maximum pixel. After candidate extraction different shape and intensity features such as area, symmetry, aspect ratio, mean contrast of edge pixels, standard deviation of edge pixels contrast, mean intensity of the microaneurysm candidate region, difference between the maximal intensity of candidate region

and local contrast and others are extracted for each microaneurysm region. After feature extraction, each microaneurysm candidate is represented by a 27 dimensional feature vector. K nearest neighbor, Adaboost and Naive Bayes classifiers are investigated and used for candidate classification.

In [21] a method for automatic detection of both microaneurysms and hemorrhages in color fundus images is described. The proposed method takes as input a color fundus image together with the binary mask of its region of interest and outputs a probability color map for red lesion detection . The region of interest is the circular area surrounded by a black background. dThe method is comprised of six steps. First, spatial calibration is applied to support different image resolutions. Second, the input image is preprocessed using smoothing and normalization. Third, the optic disc is automatically detected, to discard this area from lesion detection. Fourth, candidate regions corresponding to potential lesions, are identified in the preprocessed image, based on their intensity and contrast. Fifth, the dynamic shape features together with color features are extracted for each candidate. Sixth, candidates are classified according to their probability of being actual red lesions. Among the candidates, several regions correspond to non-lesions, such as vessel segments and remaining noise in the retinal background. To discriminate between these false positives and true lesions, an original set of dynamic shape features is presented, mainly based on shape information. In a topographic representation of the preprocessed image, each candidate corresponds by analogy to a water source. Morphological flooding is applied to the preprocessed image starting from the lowest water source and ending when the retinal background is reached. It is hypothesized that when the flooding reaches the retinal background intensity, the catchment basins degenerate and no longer contextually represent a red lesion. At each flooding level relative area, elongation, eccentricity, circularity, rectangularity and solidity are extracted. A random forest classifier is used to classify each red lesion candidate.

2.3 Detection of exudates

The exudates are lipid formations leaking from weakened blood vessels and appear as bright, yellowish structures and represent one the most important pathological structures present in patients with diabetic retinopathy. In the literature, different methods for exudate detection can be found.

For example, in [24] authors present a method for exudate detection based on improved Otsu thresholding and support vector machines. The method starts by taking the green channel of a color fundus image. Then, the image is segmented by a improved Otsu thresholding procedure. This thresholding method combines inner-cluster variance and between-cluster variance of adaptive thresholding segmentation. The optimal threshold is found by maximizing

the between-cluster variance and minimizing the inner-cluster variance. After thresholding, exudate candidate regions are obtained. After that, different features for each exudate region are extracted. In order to select the most discriminative features for exudate detection logistic regression is used. Finally, selected features are used as inputs to the support vector machines classifier.

In [25] authors present a method for detection of exudate areas, which consists of four steps. Because the method was developed using multiple datasets the first step was to standardize the image resolution across different datasets. The field of view was automatically extracted and resized to 650 pixels in diameter. Next, three lesion detection and classification algorithms are applied to the images for the detection and classification of:

- bright appearing lesions [26], i.e. hard exudates, cotton wools spots and drusen
- drusen [27]
- red lesions [28] i.e. microaneurysms and hemorrhages

In the third step, results of these systems, consisting of the detected lesions and their associated posterior probability of being a true lesion, are combined. After removing lesions with a low posterior probability, the detected lesions are used as inputs to the spatial pyramid framework by creating histograms encoding the lesion probability for each of the different type of detected lesions. Red lesion information is also included as the presence of red lesions is considered to be an indicator of diabetic retinopathy, and therefore bright appearing lesions are more likely to be exudates. Finally, a multi-class classification is obtained by using a random forest classifier in a one-versus-all classification scheme using the spatial pyramid features.

In [29] a method for detection of exudates without a manually labeled training set is presented. The method starts with background estimation using a large median filter. This estimated image is enhanced by morphological reconstruction. After that, the estimated background is subtracted from the original image in order to enhance the image. In this new image, dark structures such as the macula region, dark lesions such as microaneurysms or hemorrhages and the vasculature are clearly distinguishable from the bright structures such as the optic nerve, bright lesions (exudates and cotton wool spots) and nerve fiber reflectance residuals. The authors apply a fixed threshold in order to get exudate candidates. The exudate detection is performed by assigning a score for each exudate candidate. The exudate candidates are selected by running a 8-neighbor connected component analysis on the exudate candidate image. The scoring is performed by Kirsch's edge detector [30] and stationary wavelet analysis.

Some additional approaches are presented in Chapter 6.

2.4 Detection of neovascularizations

We explained different methods for detection of normal and pathological structures but worst cases of diabetic retinopathy are caused by neovascularizations. In this pathology, new blood vessels grow due to extensive lack of oxygen in the retinal capillaries. There is not much research on this topic in the literature.

In [22] authors present a method for detection of neovascularizations, which starts with color normalization and contrast enhancement. This is done in order to be able to detect the smallest blood vessels. The method then proceeds with blood vessel extraction step. In this step, a matching based filtering technique was applied. By using a matched filtering kernel, only regions, which property match to the kernel were enhanced. Multiple morphological operations were applied in order to remove blood vessels. After blood vessel branches were obtained, a thresholding process was carried out. After blood vessel detection, a neovascularization classification step was performed. Neovascularization classification method was constructed based on two assumptions. It is assumed that when a square window is passed through the neovascularization region, it will contain a greater number of blood vessels compared to non-neovascularization regions. Another assumption is that when a square window is passed through a neovascularization region, it will contain greater area of blood vessels compared to non-neovascularization regions. The method achieves 63.9% sensitivity and 89.4% specificity.

In [23] authors present a method for abnormal blood vessel detection and grading of proliferative diabetic retinopathy using multivariate m-mediods based classifier. The method performs preprocessing, blood vessel segmentation and optic disc localization. After that, a detailed feature set to differentiate between normal and abnormal vascular segments is extracted using different features. A new multivariate m-mediods based modeling and classification approach is then used for accurate classification of vascular segments. Finally, the system grades the fundus image as normal, neovascularizations present on optic disc or neovascularizations present elsewhere using optical disc coordinates as the output of classification process.

Chapter 3

Framework for validation of retinal segmentation methods

In order to perform method development and evaluation an image database is required. The database should have sufficient data points to be able to perform statistical analysis of results. The database should have all normal and pathological structures segmented by multiple experts in order to remove the potential bias arising from the labeling procedure.

3.1 Overview of existing databases

Before presenting our image database, which was used for testing and development of segmentation methods an overview of publicly available databases is given.

3.1.1 DRIVE database

The DRIVE (Digital Retinal Images for Vessel Extraction) is a publicly available database, consisting of a total of 40 color fundus photographs [31]. The photographs were obtained from a diabetic retinopathy screening program in the Netherlands. The screening population consisted of 400 subjects between 25 and 90 years of age. Each image has been JPEG compressed, which is common practice in screening programs. Of the 40 images in the database, 7 contain pathology, namely exudates, hemorrhages and pigment epithelium changes. The images were acquired using a Canon CR5 non-mydriatic 3-CCD camera with a 45° field of view (FOV). Each image was captured using 8 bits per color plane at 768×584 pixels. The FOV of each image was circular with a diameter of approximately 540 pixels. The set of 40 images was divided into a test and training set both containing 20 images. Three observers, the first and second author and a computer science student manually segmented a number of images. All observers were trained by an experienced ophthalmologist (the last author). The first observer segmented 14 images

of the training set while the second observer segmented the other 6 images. The test set was segmented twice resulting in a set X and Y. Set X was segmented by both the first and second observer (13 and 7 images, respectively) while set Y was completely segmented by the third observer. The performance of the vessel segmentation algorithms was measured on the test set. In set X the observers marked 577,649 pixels as vessel and 3,960,494 as background (12.7% vessel). In set Y 556,532 pixels were marked as vessel and 3,981,611 as background (12.3% vessel). This database does not contain annotated pathologies and other fundus structures like optic disc and macula.

3.1.2 STARE database

The STARE database contains 20 images for blood vessel segmentation; ten of these contain pathology [32]. The slides were captured by a Topcon TRV-50 fundus camera at 35° field of view. Each slide was digitized to produce a 605×700 pixel image, 24 bits per pixel (standard RGB). Two observers manually segmented all the images. On average, the first person labeled 32,200 pixels in each image as vessel, while the second person labeled 46,100 pixels in each image as vessel. A subsequent review indicated that the first person took a more conservative view of the boundaries of vessels and in the identification of small vessels than the second person. Performance was computed with the segmentation of the first observer as the ground truth.

3.1.3 ARIA online

This database was created in 2006, in a research collaboration between St. Paul's Eye Unit, Royal Liverpool University Hospital Trust, Liverpool, UK and the Department of Ophthalmology, Clinical Sciences, University of Liverpool, Liverpool, UK [33]. The database consists of three groups; the first group has 92 images with age-related macular degeneration, the second group has 59 images with diabetes and the control group consists of 61 images. The trace of blood vessels, the optic disc and fovea location was marked by two image analysis experts as the reference standard. The images were captured at a resolution of 768×576 pixels in RGB color with 8-bits per color plane with a Zeiss FF450+ fundus camera at a 50° FOV and stored as uncompressed TIFF files.

3.1.4 ImageRet

The ImageRet database was made publicly available in 2008 and is subdivided into two sub-databases, DIARETDB0 and DIARETDB1 [34]. DIARETDB0 contains 130 retinal images of which 20 are normal and 110 contain various signs of diabetic retinopathy. DIARETDB1

contains 89 images out of which 5 images represent healthy retinas while the other 84 have some diabetic retinopathy signs. The images were acquired with a 50° FOV using a fundus camera at a size of 1500×1152 pixels in PNG format. The images were annotated by four experts for the presence of microaneurysms, hemorrhages, and hard and soft exudates. Annotated images from four experts were combined to produce a single ground truth image. There are no manually segmented vessel images in this database.

3.1.5 Messidor

The Messidor-project database, with 1200 retinal images, is the largest database currently available on the internet and is provided by the Messidor program partners [35]. The images were acquired by 3 ophthalmologic departments using a color video 3CCD camera on a Topcon TRC NW6 non-mydriatic camera with a 45° FOV. The images were captured using 8 bits per color plane at 1440×960, 2240×1488, or 2304×1536 pixels. 800 images were acquired with pupil dilation (one drop of Tropicamide at 0.5%) and 400 without dilation. The reference standard provided contains the grading for diabetic retinopathy and the risk of macular edema in each image. This database does not contain any other annotations and is used to facilitate studies on computer-assisted diagnoses of diabetic retinopathy.

3.1.6 Review

The Retinal Vessel Image set for Estimation of Widths(REVIEW) was made available online in 2008 by the Department of Computing and Informatics at the University of Lincoln, Lincoln, UK [36]. The dataset contains 16 mydriatic images with 193 annotated vessel segments consisting of 5066 profile points manually marked by three independent experts. The images were chosen to assess the accuracy and precision of the vessel width measurement algorithms in the presence of pathology and central light reflex. The 16 images are subdivided into four sets, the high resolution image set (HRIS, 8 images), the vascular disease image set (VDIS, 4 images), the central light reflex image set (CLRIS, 2 images) and the kickpoint image set (KPIS, 2 images).

3.1.7 ROC microaneurysm set

The Retinopathy Online Challenge microaneurysm dataset is part of a multi-year online competition of microaneurysm detection that was arranged by the University of Iowa in 2009 [37]. The set of data used for the competition consisted of 50 training images with available reference standard and 50 test images where the reference standard was withheld by the organizers. The images were captured using a Topcon NW100, a Topcon NW200 or a Canon CR5-45NM

non-mydriatic camera at 45° FOV and were JPEG compressed in the camera. There are three different image sizes present in the database; 768×576, 1058×1061 and 1389×1383 pixels.

3.1.8 VICAVR

The VICAVR database is a set of retinal images used for the computation of the A/V ratio [38]. The database currently includes 58 images. The images were acquired with a Topcon NW-100 non-mydriatic camera and are optic disc centered with a resolution of 768×584. The database includes the caliber of the vessels measured at different radii from the optic disc as well as the vessel type (artery/vein) labeled by three experts.

3.2 Dibetic retinopathy image database (DRiDB)

The analysis of the publicly available databases represented a motivation for creation of a comprehensive database with the following properties:

- all fundus structures and pathologies are annotated
- at least five experts have annotated each patient image
- at least fifty patients included for statistically valid evaluation of image analysis method
- categorization of disease grade for each patient image

The images for the new database were taken and selected by medical experts from a university hospital in Zagreb. The distribution of patients does not correspond to any typical population. The diabetic retinopathy signs present vary from almost non existent to cases where new fragile vessels are visible and represent an eye sight threatening state.The images were captured at a resolution of 720×576 pixels in RGB color with 8-bits per color plane with a Zeiss VISUCAM 200 fundus camera at a 45° FOV and stored as uncompressed BMP files. Images were captured with varying flash intensities. The images contain a varying amount of image noise but we can say that images correspond to a good practical situation where the images are comparable and can be used to evaluate the general performance of diagnostic methods.

An example of an image from the database is visible inFig. 3.1.

A set of ground truth images accompanies every color fundus image from the database. For each image from the database five experts independently marked diabetic retinopathy findings. A person with a medical education and specialization in ophthalmology is considered as an expert. A special software was given to the experts to inspect the fundus images and annotate the findings.

The experts were first asked to mark the areas related to microaneurysms, hemorrhages, hard and soft exudates. These structures are not present in each image and are important because they can be used not just to measure the performance of image processing and analysis algorithms

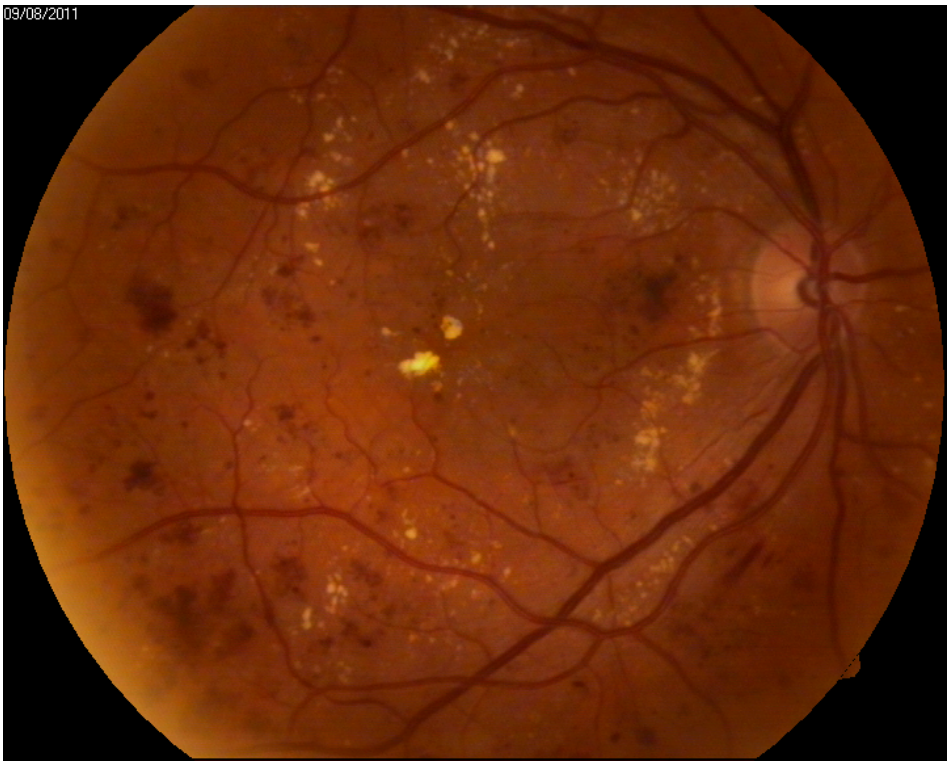

Fig. 3.1: Image from the new created database

developed for detection of diabetic retinopathy symptoms but they can be used for construction of machine learning based image processing and analysis algorithms. An example of hard exudates segmented by one of the experts and superimposed on the original image is shown in Fig. 3.2.

The experts were asked to mark the blood vessels, optic disc and the macula alongside above mentioned diabetic retinopathy signs. Segmenting those structures is important because this information can be used to improve the accuracy and robustness of image processing and analysis algorithms for detection of diabetic retinopathy pathologies. For example, we can consider an algorithm for hemorrhages detection in color fundus images. Typically, hemorrhages are darker than surrounding background but blood vessels are similar and they are darker than surrounding background too. A typical hemorrhage detection algorithm starts with blood vessel suppression because we want to eliminate similar structures but in order to do this we need to have a vessel detection and extraction algorithm. This is a different problem in comparison to our starting problem and we want to build an algorithm which can detect vessels with high accuracy. There are many different algorithms available for this type of problem but we need a good database which contains manually segmented blood vessels like the DRIVE or STARE database to test the accuracy of proposed vessel detection method. Those databases are good for vessel detection algorithms but they do not contain annotations of diabetic retinopathy pathologies like hemorrhages so the testing results obtained on those databases are sometimes not representative because for example the DRIVE database mainly consists of healthy patients with no signs of

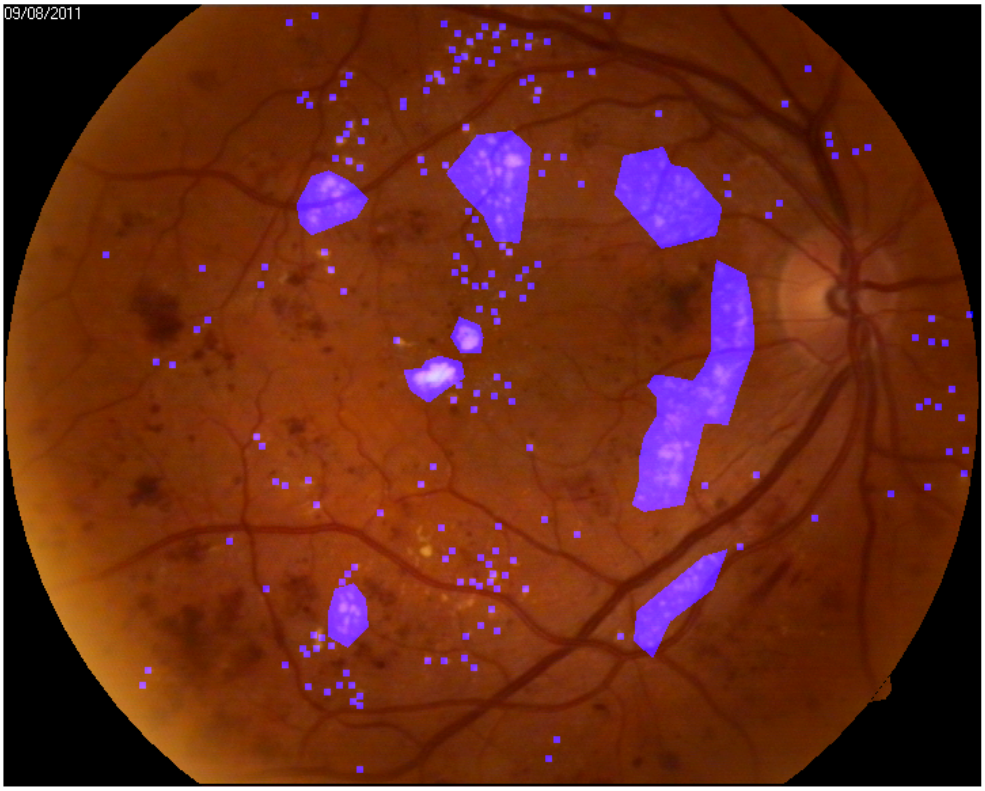

Fig. 3.2: Original image with exudates superimposed

hemorrhages and performance of vessel detection algorithms in presence of hemorrhages can be lower if we compare it to performance when no hemorrhages are present. This is the main reason why our database contains manually segmented blood vessels because we wanted to build a new database where comparison of different algorithms used in process of diabetic retinopathy pathologies detection can be reliably measured and compared. Segmented blood vessels can be used to compare the hemorrhage detection algorithms by masking out blood vessels if we want to compare different methods regardless of vessels present in the image. An example of a segmented vessel image is visible in Fig. 3.3.

In the third step the experts performed annotation of neovascularizations. A neovascularization represents a serious eye sight threatening state and may cause sudden loss in visual acuity or even a permanent blindness if not treated accordingly. In fundus images, neovascularizations appear as erratic blood vessels without any obvious direction.

Finally, each expert had to provide grading for diabetic retinopathy for each image from the database like in the Messidor database. The experts were instructed to report their confidence for each visual marking. The ground truth confidence levels available are low confidence, medium confidence and high confidence and they represent the certainty of the decision that a marked finding is correct. The experts were taught how to use the image annotation tool but they were

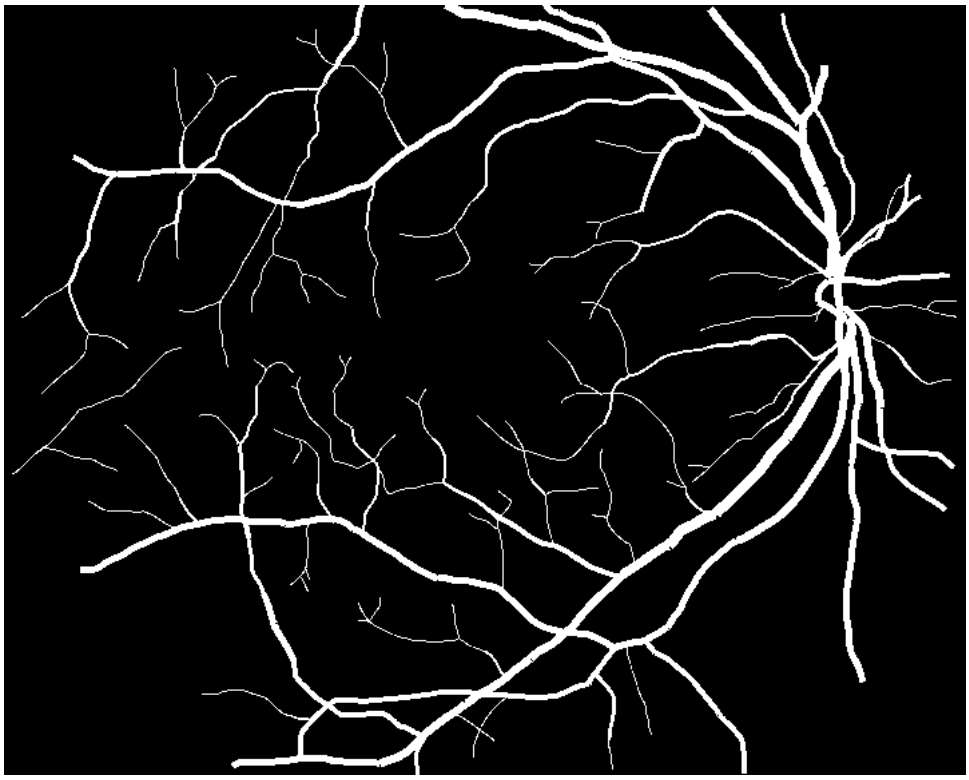

Fig. 3.3: Segmented vessel image from one of the patients

not instructed how to mark their findings to reduce biases introduced by the labeling procedure.

The created database has 50 color fundus images of which 36 contain signs of the diabetic retinopathy and 14 which do not contain any signs of the diabetic retinopathy according to all experts who participated in the evaluation.

Because blood vessels differ from other structures the image annotation tool can be actually divided into two tools. The first tool is used to mark microaneurysms, hemorrhages, hard exudates, soft exudates, macula and optic disk. The image annotation tool supports the following graphical directives:

- Centroid
- Polygon region
- Ellipse region

The centroid item is typically used to mark microaneurysms because they can be represented with a single point. The ellipse region is typically used to mark the optic disk and macula because they appear as round structures in fundus images. The polygon region is typically used for clusters of exudates and hemorrhages but the expert can use any of mentioned tools for any visual findings as he deems necessary.

Because some of the visual markings are more visible in the red-free images the expert can change the annotated image from color to red-free fundus image during the annotation procedure.

The second tool which was available to the experts was used for blood vessel segmentation and to mark neovascularizations. It is used for neovascularizations because neovascularizations are actually blood vessels so it was natural to use the blood vessel segmentation tool for this task. The tool is actually a modified version of the Live-Vessel software [39]. Using this software the user opens up an image, clicks the starting seed point of a vessel, and points the mouse to the end of the vessel. Also, the user can change the offered starting thickness of the blood vessel. The software automatically calculates the best vessel path from the seed point to the mouse position. As the user moves the mouse, the vessel is updated allowing user to control the accuracy of the segmentation with minimal effort. Usage of this annotation tool reduced the labeling time drastically because the alternative would be to mark each vessel pixel individually, which would be an extremely time consuming and tedious process.

Chapter 4

Optic disc detection using a voting based classifier and stochastic learning

The optic disc is usually visible as a bright, round structure with many blood vessels converging to this point. In Fig. 4.1 we can see a typical optic disc region marked in green. The optic disc often serves as a landmark point for other fundus features. In [40], the authors used the optic disc location as *a priori* knowledge to help estimate the location of the macula because of the relatively constant distance between the optic disc and the macula region. The optic disc can also be used as an initial point for retinal vasculature tracking methods [41]. Large vessels found in the optic disc vicinity can serve as seeds for vessel tracking methods [42]. Identifying and removing the optic disc can improve the classification of exudate regions due its similarity to yellowish exudates. The optic disc dimensions can be used to measure abnormal features of certain retinopathies, such as diabetic retinopathy and glaucoma, because the change in the shape, color or depth of the optic disc is an indicator of various pathologies such as the diabetic retinopathy and glaucoma [43].

In the literature, several optic disc algorithms can be found [44, 45, 46, 47, 48, 49, 50]. Most of them try to find the optic disc based on color, shape, brightness or some other similar features. These algorithms work very well when they are applied to healthy patients with no changes in fundus photographs. But if applied to images of low quality or images with a lot of visible artifacts their accuracy decreases.

In order to increase the accuracy of optic disc detection we combine several optic disc detection algorithms into an ensemble. First, we apply each optic disc detection algorithm to the input image and obtain optic disc probability maps for each algorithm applied. Then, we combine these probability maps into a single probability map and find the point, which has the highest probability of being a point inside the optic disc. This simple procedure increases the accuracy of optic disc detection compared to individual optic disc detection algorithms. The flowchart of the proposed method is visible in Fig. 4.2.

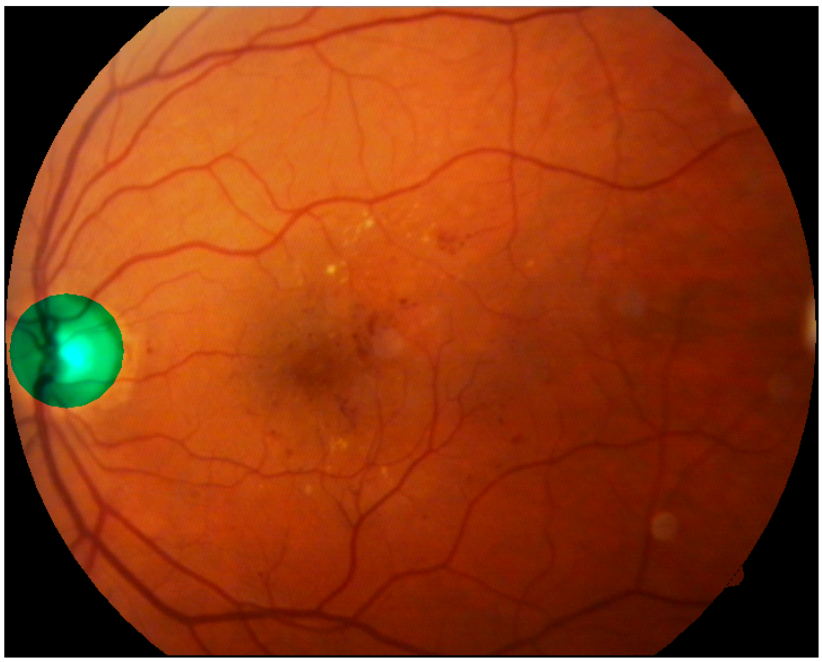

Fig. 4.1: A fundus image with optic disc marked

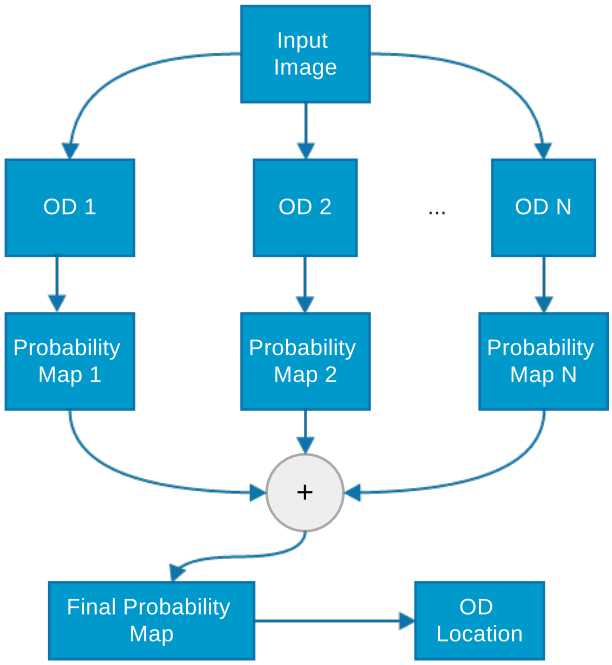

Fig. 4.2: Flowchart of the proposed optic disc detection method

4.1 Individual optic disc detection algorithms

In this section we give a short description of optic disc detection methods, which we used in order to create the ensemble. We implemented seven different methods described in the literature.

4.1.1 Hough transformation of vessels approach

In [46] the authors propose a method which uses Hough transformation on the thinned vessels. The method starts with blood vessel detection. The performance of the blood vessel detection method is not crucial for the performance of this method because only thick vessels near the optic disc have to be segmented in order for the method to work properly. After thresholding, morphological thinning is performed. The thinning operation is performed in order to approximate each vessel with a line segment. After thinning, Hough transform [51] is applied to the binary image. After performing the Hough transform, lines, which have a slope smaller than 45° are removed. For each line pair, intersection points are found and a vote is cast at the intersection point resulting in a voting map. If the intersection point is located outside of the image no votes are cast. Values in the voting field represent the number of line pairs intersecting at that point. In order to spread the influence of the voting to the surrounding area, a circular mean filter of size 5×5 is applied to the voting field. Because the optic disc is one of the brightest areas of the fundus image, the voting field values are weighted by the intensity values located at the intersection points in the original image. The weights were empirically found and were set to 0.7 for voting field and 0.3 for the brightness level of each pixel. In this approach the highest value would represent the center of the optic disc, but we do not want the optic disc position but a probability map of pixel being an optic disc center so we normalize the voting values to 0-1 range.

4.1.2 Pyramidal decomposition approach

Pyramidal decomposition can be used to detect large areas of bright pixels that probably represent the optic disc. Because the pyramidal decomposition can be easily fooled by large areas of bright pixels that may occur near the image borders due to uneven illumination in [49] authors first perform illumination equalization of the green channel in order to decrease the effects of uneven illumination present in such images. After illumination equlization, resolution pyramid is created using a simple Haar-based discrete wavelet transform citechen1997haar. At the fifth level of the resolution pyramid, the small bright pixels belonging to exudates disappear but the optic disc is still visible. In the proposed method the brightest pixel at the fifth level would be selected as the optic disc area in the original image but because we want the probability map we just upscale the downscaled image to the original size and normalize it to the 0-1 range.

4.1.3 Vessel direction matched filtering (VDM) approach

In [47] the authors propose a simple vessels direction matched filtering approach. The algorithm starts by performing illumination equalization of the green channel and finds the blood vessels using a simple edge fitting algorithm proposed by [52]. The binary vessel image is thinned,

and all remaining vessel-labeled pixels that are not within 41×41 square centered on each of the highest 4% intensity pixels in the illumination equalized image are relabeled as non-vessel pixels. In the final step a direct matched filter is applied to roughly match the direction of the vessels at the optic disc vicinity. The output of the matched filter, which represents the optic disc location is normalized to 0-1 range in order to obtain the probability map.

4.1.4 Fuzzy convergence approach

In [45] the authors propose an optic disc detection method based on a fuzzy voting mechanism. The method tries do find the blood vessel origination point and in this way finds the optic disc as the point of blood vessel origination. The inputs to the algorithm are six segmented binary vessel images obtained from the green channel of the input image each taken at a different scale. The binary vessel images are obtained by thresholding the images obtained using Frangi vesselness [53] filter. After thresholding, the binary images are thinned to one pixel width. Branch points are relabeled as background, thus breaking up the vessels into segments, which contain two end points each. Each thinned vessel is defined with two endpoints (x_1, y_1) and (x_2, y_2) and is modeled by a fuzzy segment model, which is defined by a set of parametric line segments:

$$x(t) = x_1 + r\cos(\alpha + \theta) + (x_2 - x_1 - 2r\cos(\theta)\cos(\alpha))t \tag{4.1}$$

$$y(t) = y_1 + r\sin(\alpha + \theta) + (y_2 - y_1 - 2r\cos(\theta)\sin(\alpha))t \tag{4.2}$$

where:

$$0 \leq t \leq 1$$
$$0 \leq \theta \leq 2\pi$$
$$0 \leq r \leq R$$

In this case, R defines the amount of fuzziness of each line segment. If this parameter is set to zero, each fuzzy segment is actually reduced to a normal line from (x_1, y_1) to (x_2, y_2). The parameter α corresponds to the orientation of the original line segmented and is calculated as:

$$\alpha = \frac{\pi}{2} - \arctan\frac{y_2 - y_1}{x_2 - x_1} \tag{4.3}$$

Using this fuzzy model it is possible to generate a voting map where each pixel equals the amount of fuzzy segments on which the pixel lies. Finally, the voting map image is smoothed using a circular 5×5 mean filter and normalized to 0-1 range in order to obtain a probability map.

4.1.5 Brightness approach

In [54] the authors propose an optic disc localization method, which uses a thresholding procedure in order to obtain pixels with high intensity values and selects the center of the largest object as the optic disc center. The detection of the optic disc is performed on the intensity component of the Hue-Saturation-Intensity image. The algorithm assumes that the optic disc is the largest and brightest part of the fundus images, which usually holds true. A fixed threshold is applied to obtain a binary image containing parts of the optic disc and perhaps other bright pathologies such as exudates. The threshold is found by first calculating the histogram of the intensity image and selecting the value for which the binary image contains the brightest two percent of pixels. The largest connected object within the thresholded image is expected to be a part of the optic disc. So we assign value one to pixels belonging to the largest connected object and value zero to all other regions in our probability map.

4.1.6 LoG filtering approach

Because we assume that the optic disc is an object, approximately circular and consisting of bright pixels, general methods for detection of blobs in grayscale images can be used [55]. In this approach, we decided to use the Laplacian of Gaussian (LoG) filtering approach [56]. We start with the green channel of the original image, and apply the Laplacian of Gaussian filter to the original image. The green channel is used because the most contrast is usually present in that channel. The convolution mask used is circular and the radius of the mask is similar to the radius of the optic disc because we want the kernel shape to be similar to the optic disc. After applying the convolution we just normalize the image to 0-1 range to obtain the optic disc probability map.

4.1.7 Entropy approach

In [50] the authors use entropy filtering for optic disc detection. Because the optic disc is the origination point of the main vessels we can expect high entropy in those areas because high entropy corresponds to areas with high local variability. The method starts by taking the original RGB image and transforming it into Hue-Saturation-Intensitiy color space where median filtering in a 5×5 window is applied to remove noise. To increase local contrast, Contrast Limited Adaptive Histogram Equalization (CLAHE) is applied to the intensity channel after noise removal [57]. After preprocessing, entropy is calculated in a small sliding window using (4.4).

$$H(I_x) = -\sum_{i=0}^{255} P_{I_x}(i) \cdot \log P_{I_x}(i) \tag{4.4}$$

Here, P_{I_x} is the probability mass function of pixel intensities I_x in a local neighborhood of x. In the paper, authors apply the Otsu's [58] binarization algorithm to separate complex regions represented with high entropy from smooth regions represented with low entropy but because we want to preserve as much information as possible we just normalize the entropy values to 0-1 range.

4.2 Combining different probability maps

In the proposed approach an improved optic detection algorithm is created by using an ensemble of seven methods described in the previous section. Each method in the ensemble generates a probability map, which defines the probability of a pixel being part of the optic disc. Information from different probability maps can be combined in different ways because we generate seven probability maps for each input image. We decided to implement a straightforward method, which constructs a new probability map by weighting different probability maps obtained by our optic disc detection methods and adding them together. The optic disc can be easily found in this new probability map by finding the maximum value in the probability map. An example of the input image and corresponding optic disc probability map is visible in Fig. 4.3 and Fig. 4.4.

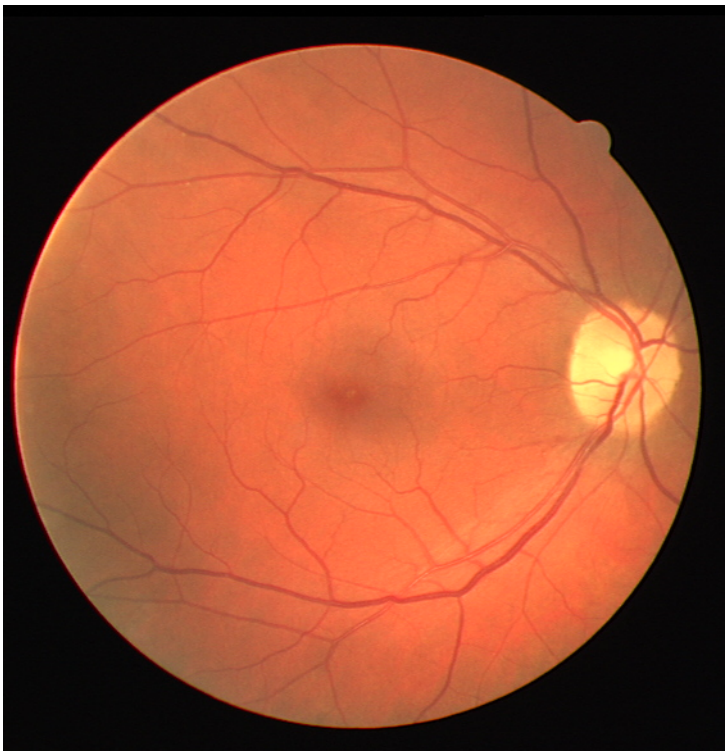

Fig. 4.3: An example image used for optic disc detection

The weights used for creation of the final optic disc probability map can be chosen in various ways. If we set each weight to $\frac{1}{N}$, where N is the number of optic disc detection algorithms,

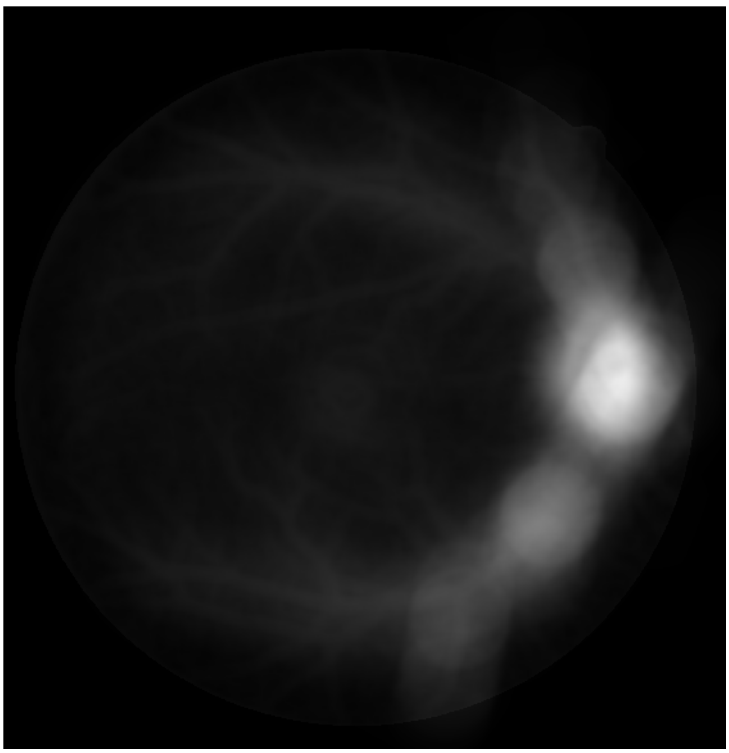

Fig. 4.4: Final optic disc probability map

this would translate into equal weighting of each method. From our experiments, we know that different methods show different accuracies we would like to find the weights, which would increase the overall accuracy of the proposed system. We decided to use the well known simulated annealing search algorithm to find the optimal weights for each probability map [59]. The energy function, which is used by the simulated annealing search algorithm, is just the number of misclassified optic disc locations. In our experiments, for each image the optic disc was manually segmented so we could easily check if the optic disc location found by each of the algorithms was correct by looking if the location was inside of the marked optic disc region.

After each step of the simulated annealing algorithm, weights in the current iteration were used to create the combined probability map. In this probability map, the optic disc location was found by looking at the maximum value in the probability map. If this location was outside of the marked optic disc mask the counter of misclassified optic locations was increased. The goal of the simulated annealing optimization procedure was to minimize the number of misclassified locations. This approach can be used for arbitrarily large number of different optic disc detection algorithms and shows improved performance compared to individual optic detection algorithms.

4.3 Performance evaluation

We have evaluated our ensemble based algorithm for optic disc detection using several publicly available database. We split the database into two disjoint sets for training and testing purposes. We need to split the database because we need training images to find the weights using the simulated annealing search algorithm. The training database contains 30% of the images from each of the databases and the test database contains the the other 70% of the images. To increase the statistical significance of the results multiple rounds of cross-validation are performed using different image database partitions, where we use different images for training and other images for testing the proposed method.

We evaluated the accuracy of the methods using a simple criterion. We count the number of fundus images in which the output of the optic disc detection algorithm falls inside the manually selected optic disc patch. Table 4.1 shows the performance of different optic disc detection algorithms compared to the proposed method.

Table 4.1: Performance of optic disc detection algorithms

Method	DiaretDB0	DiaretDB1	DRIVE	DRiDB
OD_{Hough}	93.00%	88.76%	95.00%	80.00%
$OD_{Pyramidal}$	93.08%	89.89%	97.50%	96.00%
OD_{VDM}	84.62%	88.76%	100%	88.00%
OD_{Fuzzy}	76.92%	78.65%	95.00%	88.00%
$OD_{Brightness}$	95.38%	95.51%	97.50%	100.00%
OD_{LoG}	87.69%	87.64%	95.00%	92.00%
$OD_{Entropy}$	93.85%	94.38%	97.50%	86.00%
Proposed	98.46%	98.88%	100%	100%

The results show that the proposed method outperforms other optic detection algorithms, which are part of the proposed ensemble. This framework is expandable and other optic disc detection algorithms can be easily added, which could probably increase the performance of the proposed method even further.

Because the DRIVE database consists of mainly high quality images the accuracy is high and doesn't represent a problem for the proposed method but so was the case for other methods. The solution can fail in cases where some other structures similar to the optic disc exist in the fundus image. This can happen if a large structure of exudates appears near the optical disc due to the fact that exudates appear as bright yellow structures, which affects the localization of the optic disc.

Chapter 5

Blood vessel segmentation from fundus photographs using model-based multi-scale vessel tracking

Blood vessel segmentation in color fundus photographs is useful for diagnosis, screening and evaluation of different cardiovascular and ophthalmic diseases such as diabetes, diabetic retinopathy, hypertension. Automating the segmentation of blood vessels is very important because manual segmentation is long and time consuming task, which requires medical knowledge and skill. In order to develop an automated screening system for early detection of diabetic retinopathy an automated blood vessel segmentation is required. In the literature, we can find many different methods and approaches for automatic detection of blood vessels in color fundus photographs. A good overview of different blood vessel detection methods is given in [7]. In the literature we can find a lot of methods based on matched filtering where the original fundus image is convolved with a 2-D kernel [10, 52, 60]. The kernel is designed to match the structure of blood vessels and typical blood vessel properties such that vessels usually have a limited local curvature, they can be approximated by piecewise linear segments and the cross-sectional pixel intensity profile of the line segment can be approximated with an inverted Gaussian curve. For example, in [52] authors use a two-dimensional linear kernel with a Gaussian profile for segmentation of retinal vessels. The profile of the filter was designed to match the Gaussian shape of the blood vessel profile. In order to detect blood vessels in all directions the kernel was rotated by 15° increments. The maximum response over all rotations is taken and the image is thresholded in order to obtain a binary image. Morphological processing based methods for blood vessel detection are also common in the literature [11, 61, 62, 63, 64]. For example, authors in [11] combined morphological multi-scale enhancement, fuzzy filtering and watershed transformation for vessel segmentation. The background is estimated by using non-linear multi-scale morphological opening operators with different structuring elements and then the

background is subtracted from the original image for contrast enhancement. Vessel tracking methods segment a vessel between two points and usually work at a vessel level and multiple start points are required to segment the whole vasculature tree. The main advantage of vessel tracking methods is that they provide accurate vessel widths and usually can give information about the structure of the whole vasculature tree. Usually, vessel tracking approaches are combined with matched filtering or morphological operators. In [65] authors used matched filtering combined with the Kalman filter in order to segment the blood vessels. First, the second order Gaussian matched filter is employed to estimate the vessel centerline and then the tracking procedure is started where the Kalman filter is employed to estimate the next vessel segment. Some authors used machine learning and classification techniques in order to segment the blood vessels [66, 67, 68]. For example, in [67] authors used a deep convolutional neural network combined with random forests. In the proposed approach outputs of the pooling layers were used as features for an ensemble of random forests. Different types of ensembles were used and impressive results were obtained both on the DRIVE [31] and STARE [32] databases. Model based approaches apply the explicit vessel models to extract the retinal vessels [12, 69, 70, 71]. In [12] authors presented a regularization based multi-concavity modeling approach, which is able to handle both normal and pathological retinas. A line shape concavity measure is used to distinguish the irregular shape intensity structure of dark lesions from the line shape intensity structure of the blood vessel. A locally normalized concavity measure is used to filter out noise. Those concavity measures are combined according to their statistical and geometrical properties. A lifting scheme is used for regularizing the solution towards the ideal vessel shape.

The method presented here builds upon the method presented in [72]. Most vessel tracking methods start with an initial point and then estimate the vessel width and orientation within a local region at the current point. After the vessel width and orientation are estimated, a small step is taken in the direction of the vessel orientation. This procedure is repeated until the full vessel is traced out.

Different methods of estimating the vessel width and orientation can be used. Some proceed by detecting the edges of the vessel closest to the current point to estimate the orientation [73]. These methods can fail or produce inaccurate results if insufficient number of edge pixels are used. Some methods try to rectify this problem by applying a convolution operation. In this case, a model of the vessel shape or two separate operators modeling the vessel edges in the neighborhood of the vessel edges are used. By applying the convolution with the model rotated at different orientations, the peak response can be used to more accurately measure the vessel orientation. Instead of applying the convolution operator at different orientations one could try to fit a model of the vessel using an optimization procedure. Using such an optimization procedure one could potentially find the orientation and width of the vessel at the given point. Using a two-dimensional model and a two-dimensional local region around the current point can

increase the accuracy and robustness of blood vessel orientation and width estimation. Such an optimization problem is highly non-linear so a good starting solution is required in order to increase the probability of proper convergence. Because vessels usually do not change the profile or orientation within a local region using such a two-dimensional model and a good starting solution increases the probability of a better solution, which enables a more accurate estimate of the next tracking point. Because a reasonable number of pixels is used for model fitting, vessels in noisy images or in low contrast regions can be properly tracked.

In our approach the optimization procedure starts with a point (x,y) on the vessel, an estimate of orientation θ and an estimate of vessel width σ. Using that information, a small region around that point is cut out and a 2D non-linear least-squares fit of the vessel model is made over the local region. This procedure increases the robustness of blood vessel width and orientation estimate. After the optimization procedure, the estimated width and orientation are used to make a small step using the estimated vessel orientation. The step is proportional to estimated width of the blood vessel. Those new estimated orientations and widths are used for the next iteration of the optimization process.

5.1 One-dimensional blood vessel models

The blood vessel model used in the non-linear optimization procedure assumes that the darker appearance of blood vessels is primary due to the attenuation of red-free light as it passes through the blood column [72]. The attenuation can be modelled according to the Bouguer's law [74], where the exit beam intensity is given by (5.1).

$$I(x) = I_0 e^{-\int \alpha(x,z)dz} \tag{5.1}$$

Here, $\alpha(x,z)$ is the linear attenuation coefficient, x is the dimension in the plane of the retina across the vessel and z is depth into the retina. If α is taken as constant throughout the vessel, and the vessel profile is said to be symmetric and circular, then the received light is defined with (5.2).

$$I(x) = I_0 \left(1 - ae^{-(x-x_0)^2/2\sigma^2}\right) \tag{5.2}$$

Here, x_0 is the center of the vessel, σ defines the width of the vessel, and a is a constant giving the relative amount of light absorbed by the vessel. Using such a model would fail to take in account the light reflex often seen in the center of the vessel. In Fig. 5.1 we can clearly see the light reflex.

According to the [75] the light reflex is explained by the scattering of light off the rough column of blood and the intravascular column of erythocytes. This scattering can also be usefully modeled by a Gaussian that is narrower and inverted compared to the simple vessel model. This

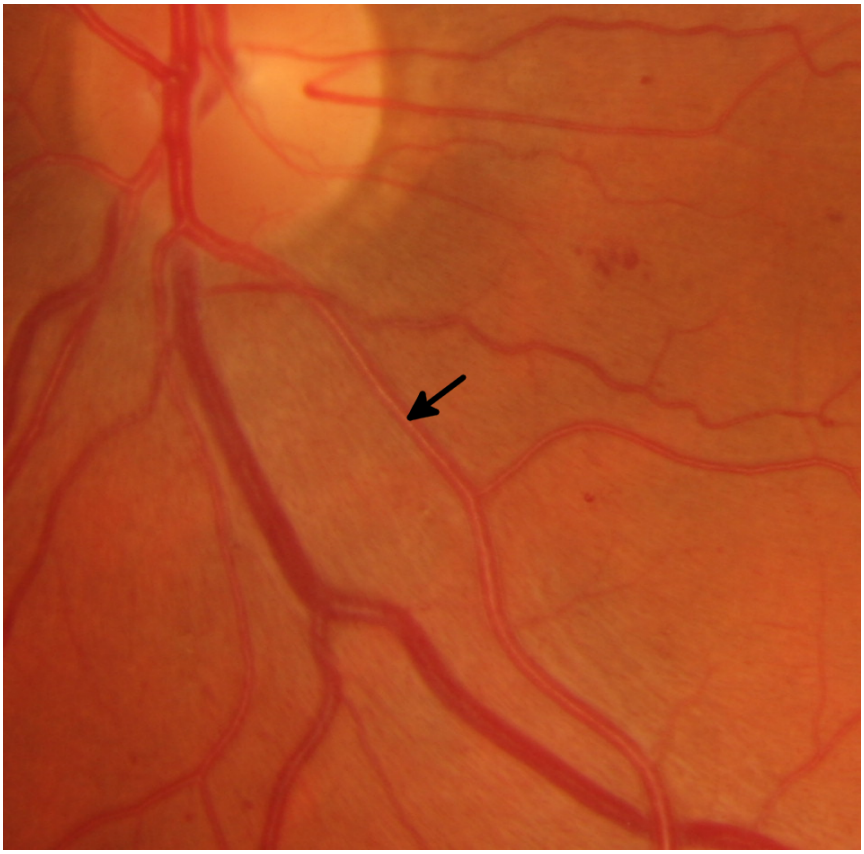

Fig. 5.1: Segment of the image with light reflex marked

reflex can than be modeled using (5.3).

$$I(x) = I_0\left(1 - ae^{-(x-x_0)^2/2\sigma^2} + be^{-(x-x_0)^2/2\sigma_r^2}\right) \tag{5.3}$$

Here, b is the relative fraction of the light reflex, and σ_r is the light reflex width where $\sigma_r < \sigma$. In [76] authors proposed another model for light reflex but instead of adding the two components together, switches for two components exist as is presented in (5.4).

$$\begin{aligned} I(x) &= I_0\left(1 - ae^{-(x-x_0)^2/2\sigma^2}\right), \quad x < P,\ x > Q \\ I(x) &= I_0 be^{-(x-x_1)^2/2\sigma_r^2} \qquad\quad , \quad P \leq x \leq Q \end{aligned} \tag{5.4}$$

Here, a and b are the relative amount of the two amount of the two components of the blood vessel, x_1 is the blood vessel center point, σ_r is the width of reflex, P and W are the cutover points between the two components.

5.2 Two-dimensional blood vessel model

Models presented here are made for 1D case, where we look at the intensity profile of the blood vessel. In order to find the width and orientation of the blood vessel, a two dimensional

model has to be used. The extension of the model is presented [72] and explained in short here. The 2D model extends the basic 1D model presented in (5.2), which explains the change the brightness level across the blood vessel. The 2D model extends the 1D model by giving the vessel an orientation in the 2D plane and extending the vessel in the direction orthogonal to its cross-section. It is assumed that the extension of the blood vessel in 2D is linear and uniform. This means that the blood vessel has the same cross section at all points along the vessel.

In order to convert the 1D vessel model to a 2D vessel model and reduce the number of optimization parameters (x,y) coordinates of the local optimization region are converted to a new coordinate space (u,v). Here, u points in the same direction as the vessel and v is orthogonal to the vessel. The connection between two coordinate spaces is given by (5.5).

$$\begin{aligned} u &= x\sin(\theta) - y\cos(\theta) \\ v &= x\cos(\theta) + y\sin(\theta) \end{aligned} \tag{5.5}$$

The vessel profile is given by the single Gaussian model presented with (5.6).

$$I(v) = A - Be^{-(v-v_0)^2/2\sigma^2} \tag{5.6}$$

Here, A is the background intensity, B is the contrast of the vessel with respect to the background intensity B, and v_0 enables the vessel center to be shifted in the v direction.

Sometimes a vessel may be tortuous and bend suddenly in a localized region. This can lead to bad optimization results or even it cause the whole fitting procedure to fail, as the assumption that the vessel cross-section can be extended linearly in one direction is violated. This problem can be solved by allowing the vessel to flex inside the optimization region. This can be achieved by adding a quadratic term in v to u so the (5.5) is extended in (5.7).

$$\begin{aligned} u &= x\sin(\theta) - y\cos(\theta) + \eta v^2 \\ v &= x\cos(\theta) + y\sin(\theta) \end{aligned} \tag{5.7}$$

Here, η describes the curvature of the vessel. If $\eta = 0$ than there is no curvature in the fitting area. If $|\eta| > 0$ then the vessel will bend in the direction of u about the origin.

5.3 Blood vessel enhancement

In order to improve the performance of the algorithm the optimization procedure is not applied to raw pixel values of the image but to the blood vessel enhanced image. A common approach for detection of linear structures is the well known Frangi vesselness filter [53]. In this appro-

ach the vessel enhancement process can be formulated as a filtering process that searches for tubular structure in images. Because blood vessels can appear in different sizes it is important to introduce a measurement scale which varies within a certain range. In order to analyze the local behavior of an Image a Taylor expansion in the neighborhood of point x_o is considered in (5.8).

$$L(x_o + \delta x_o, s) \approx L(x_o, s) + \delta x_o^T \nabla_{o,s} + \delta x_o^T H_{o,s} \delta x_o \tag{5.8}$$

This expansion approximates the structure of the image up to second order. $\nabla_{o,s}$ and $H_{o,s}$ are the gradient vector and Hessian matrix of the image computed in x_o at scale s. In the linear scale space theory framework explained in [77, 78] the differentiation operator is defined as a convolution with derivatives of Gaussians as visible in (5.9).

$$\frac{\partial}{\partial x} L(x,y) = s^{\gamma} L(x) * \frac{\partial}{\partial x} G(x,s) \tag{5.9}$$

Here, the D dimensional Gaussian is defined as (5.10).

$$G(x,s) = \frac{1}{\sqrt[D]{2\pi s^2}} e^{-\frac{||x||^2}{2\sigma^2}} \tag{5.10}$$

The parameter γ was introduced in [79] to define a family of normalized derivatives. This normalization is particularly important for a fair comparison of the response of differential operators at multiple scales. Analyzing the second order information embedded in the Hessian matrix can be used in the context of blood vessel detection. The second derivative of a Gaussian kernel at scale s generates a kernel mask, which when applied to the image measures the contrast between the regions inside and outside of the range $(-s, s)$ in the direction of the derivative. The third term from (5.8) is actually the second order directional derivative (5.11).

$$\delta x_o^T H_{o,s} \delta x_o = \left(\frac{\partial}{\partial \delta x_o} \right) \left(\frac{\partial}{\partial \delta x_o} \right) L(x_o, s) \tag{5.11}$$

The analysis of the Hessian matrix is useful because after extracting the eigenvalues and eigenvectors of the Hessian matrix this information can be used to directly obtain the direction of the smallest curvature. In areas, which contain blood vessels, the direction of the smallest curvature is along the vessel. This procedure avoids applying several filters in multiple directions because applying multiple filters is much more computationally expensive and requires a discretization of the orientation space. For simplicity, let $|\lambda_1| \leq |\lambda_2|$ denote the two eigenvalues of the Hessian matrix and $\mathbf{u_1}$, $\mathbf{u_2}$ the corresponding eigenvectors. Since λ_1 is the eigenvalue with the smallest magnitude, the eigenvector $\mathbf{u_1}$ points in the direction of the smallest curvature, λ_2 corresponds to the eigenvector $\mathbf{u}_2$, pointing in direction of the largest curvature. For vessel points this means that eigenvector $\mathbf{u_1}$ points along the vessel and the corresponding eigenvalue

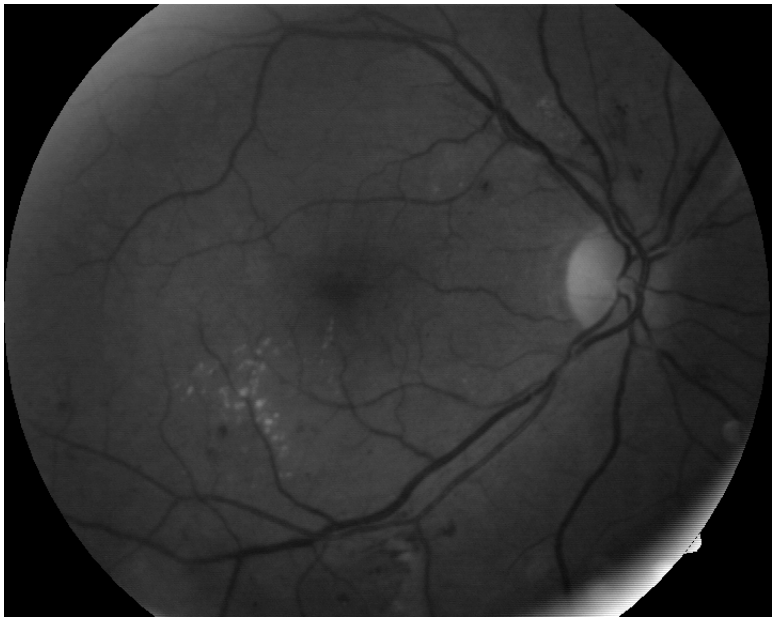

(a) Original image

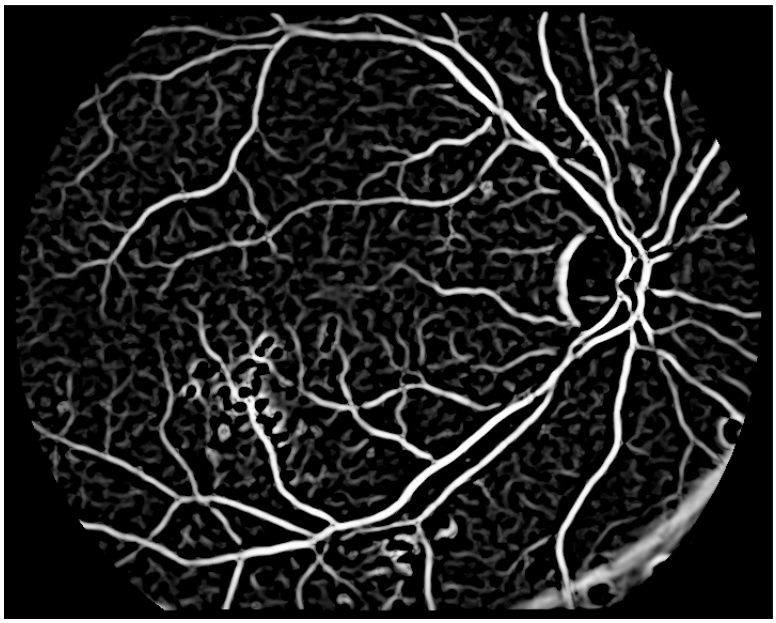

(b) Output of the Frangi vesselness measure for selected scale

Fig. 5.2: Example of the Frangi vesselness filtering

λ_1 should be close to zero. This also means that the eigenvector $\mathbf{u_2}$ points towards the edge of the blood vessel and the corresponding eigenvalue λ_2 is large in magnitude. The Frangi vesselness measure combines this observation to create a response, which should be high in areas belonging to blood vessels and low in other areas. In order to incorporate this information two

measures are defined in (5.13), which capture the anisotropy and contrast of the given pixel.

$$R_b = \frac{|\lambda_1|}{|\lambda_2|} \tag{5.12}$$

$$S = ||H|| = \sqrt{\lambda_1^2 + \lambda_2^2} \tag{5.13}$$

For blood vessel pixels R_B should be low because λ_1 should be close to zero in magnitude and λ_2 should be large in magnitude. S will be low if both the eigenvalues are small for the lack of contrast so that the larger S is the more likely it is a blood vessel. For images where the vessels are darker than their background, meaning that the vessels are valleys, the curvature will be negative so $\lambda_2 < 0$. Using this information, the Frangi vesselness output can be expressed using (5.14).

$$\begin{aligned} F(x,y) &= 0 \qquad\qquad\qquad , \quad \text{if } \lambda_2 > 0 \\ F(x,y) &= e^{-\frac{R_b^2}{2\alpha^2}} \left(1 - e^{\frac{S^2}{2\beta^2}}\right), \quad otherwise \end{aligned} \tag{5.14}$$

Here, α and β are parameters to adjust the effect of R_b and S. Because the second order Gaussian derivative can be calculated at different scales s there are multiple responses of the vesselness filter for each pixel. Usually, the maximum value response over the scales can be used to create a single vesselness output. Here, this is not done in order to preserve the information about the scale at which the maximum was obtained. This information is then used in the tracking phase of the algorithm. In Fig. 5.2 we can see the original image and the corresponding vesselness response image.

5.4 Blood vessel tracking

Given a seed point, the scale with the maximum vesselness is taken as the starting estimate of the blood vessel width. In the vesselness calculation stage, information about the vessel orientation is obtained by looking at the eigenvector corresponding to the smallest eigenvalue. This eigenvector points in the vessel direction and is used as a start estimate of the blood vessel orientation. The start estimate of the blood vessel orientation is used in order to cut out the fitting region in the blood vessel direction. The region for fitting is defined by taking 2 ceil$(2\sigma)+1$ pixels along the u axis and 2 ceil$(\frac{3}{2}\sigma)+1$ pixels along the v axis. The local region has to be oriented with the vessel in order to enable more robust estimate of the parameters. Because the scale with the largest vesselness response is known, the region is cut from the vesselness measure at that scale. Optimization is done by the standard non-linear Marquardt [80] algorithm.

After the optimization step is performed, a new estimate of the blood vessel orientation and width is obtained. This estimate is then used to move to the next point. The next point where

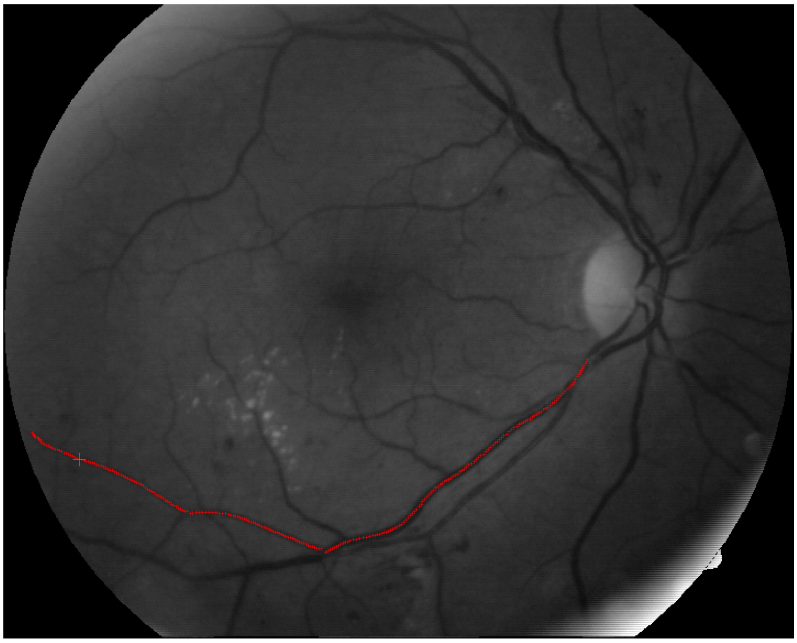

Fig. 5.3: Example of blood vessel tracking. The tracked points are marked with red and the starting seed point with green

the fitting procedure continues is found using (5.15).

$$\begin{aligned} x_{new} &= x_{old} + cos(\theta_e) * \sigma_e * a \\ y_{new} &= y_{old} + sin(\theta_e) * \sigma_e * a \end{aligned} \tag{5.15}$$

Here, θ_e is the estimate of the blood vessel orientation found using the optimization procedure applied in (x_{old}, y_{old}), σ_e is the estimate of the blood vessel orientation found using the optimization procedure applied in (x_{old}, y_{old}) and a is a small constant defining the amount of movement in the blood vessel direction. After this step, a new region is cut out and the optimization procedure is repeated. The new blood vessel width estimate is used to select the proper vesselness map. The vesselness map, which was generated using the σ value closest to the estimated blood vessel width is used to cut the fitting region. After the optimization procedure fails the optimization procedures restarts at the same seed point but the tracking direction is reversed. This is achieved by applying (5.16) instead of (5.15).

$$\begin{aligned} x_{new} &= x_{old} - cos(\theta_e) * \sigma_e * a \\ y_{new} &= y_{old} - sin(\theta_e) * \sigma_e * a \end{aligned} \tag{5.16}$$

In Fig. 5.3 an example of a tracked line is visible in red with the seed point marked with a large green cross.

5.5 Seed point generation

Before the tracking procedure can start seed points have to be generated. The seed points are generated using the vesselness information. First, the maximum over all scales is taken, which creates a grayscale image. In this images, higher values should represent higher blood vessel probabilities. In order to have a uniform distribution of seed points across the whole image, the vesselness images is divided in $m \times m$ non overlapping square blocks. In each block, k points with highest vessleness values are chosen as the the seed points. In Fig. 5.4 image with seed points superimposed is visible. Values for m and k were found empirically.

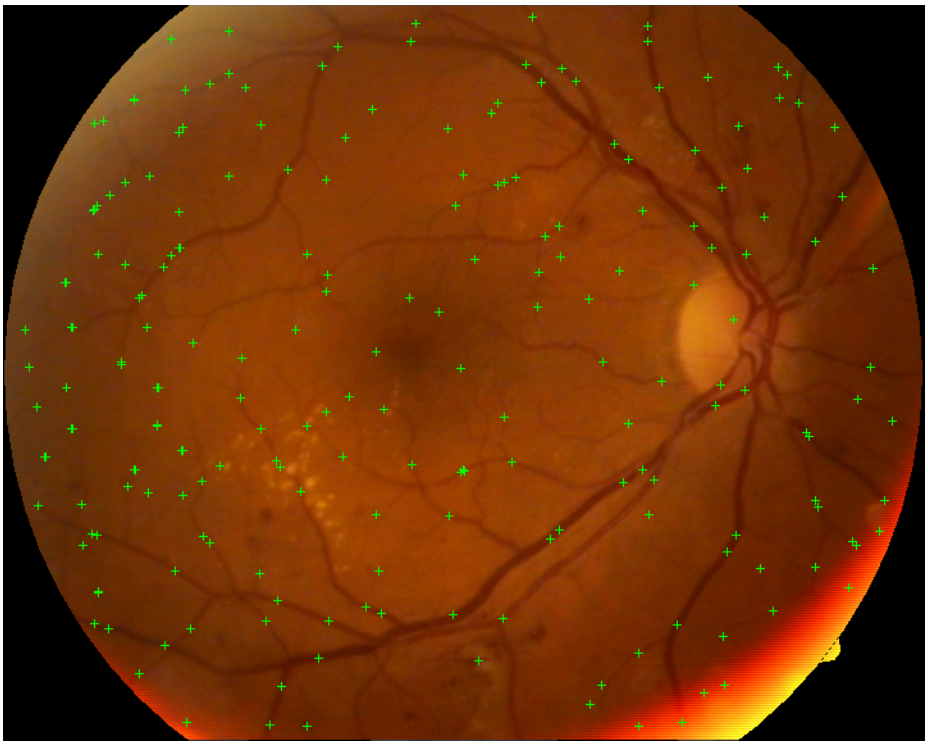

Fig. 5.4: Example of seed points used for blood vessel tracking

5.6 Performance evaluation

In order to quantitatively measure the performance of the proposed method we calculate the accuracy, true positive rate (TPR) and false positive rate (FPR). TPR represents the fraction of pixels correctly detected as vessel pixels and is given by (5.17),

$$TPR = \frac{TP}{TP + FN} \tag{5.17}$$

FPR is the fraction of pixels erroneously detected as vessel pixels and is given by (5.18).

$$FPR = \frac{FP}{TN + FP} \tag{5.18}$$

The accuracy is measured by the ratio of the total number of correctly classified pixels to the number of pixels in the image field of view. The method achieves an average accuracy of 0.9436 with 0.7134 and 0.0415 TPR and FPR, respectively on the DRIVE database [31].

In Fig. 5.5 we can see the original, ground truth image and result of our vessel tracking method.

(a) Original image

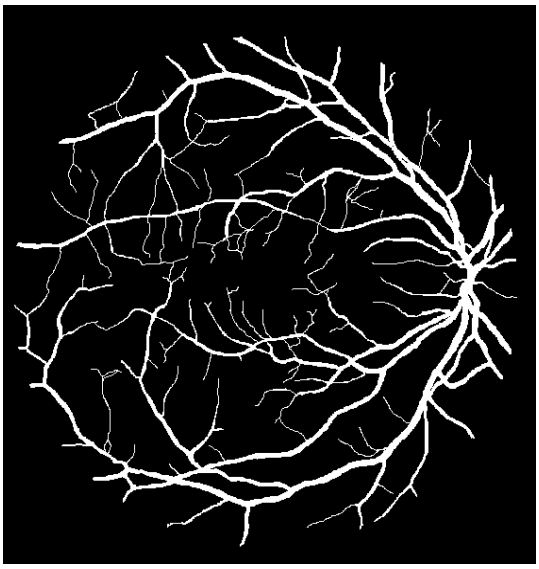

(b) Ground truth data

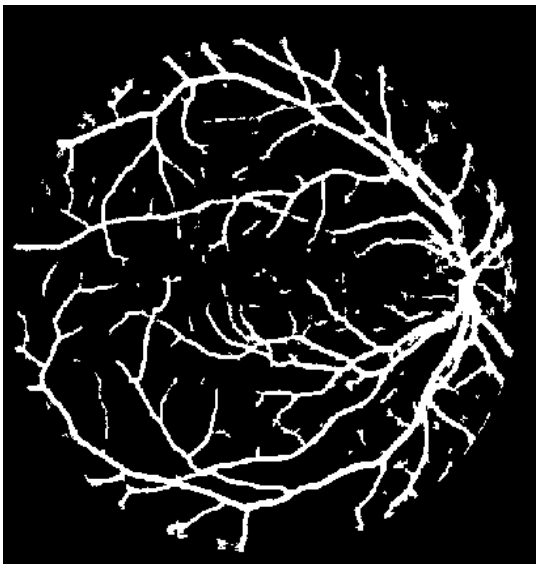

(c) Output of our blood vessel segmentation method

Fig. 5.5: Example of blood vessel tracking

From the example image we can clearly see that the method can generate reasonably accurate segmentation of the blood vessel network. Compared to the ground truth segmentation we can notice some pixels marked as blood vessels although they are clearly not blood vessels. Those false positive pixels usually appear due to bad initialization of the tracking procedure. Because we want to detect as many thin vessels as possible we need to have a large number

of seed pixels because tracking can fail due to any number of reasons such as low contrast, complicated branching, edge of the blood vessel etc. Because the seed points can be wrongly initialized, in some case the tracked points do not represent the actual blood vessel network. This happens because the optimization model assumes that darker linear structures are blood vessels, which can be problematic if other similar structures are present in the image but don't represent blood vessels.

Chapter 6

Exudate detection using voting-based classifier and stochastic learning

In the literature, we can find many different techniques for automatic detection of diabetic retinopathy pathologies in color fundus photographs such as exudates. Most of the methods start with some sort of image preprocessing, followed by exudate candidate extraction procedure where a set of exudate candidates, i.e. structures, which are exudates or which are similar to exudates are extracted. In order to segment all exudate regions large number of non-exudate regions are also segmented. Finally, a classification step is applied, where different features are extracted for each exudate candidate in order to keep the real exudate areas only. The final classification step reduces the number of false positives, i.e. the goal of this step is to discard regions which are not actually exudates but were selected in the candidate extraction step.

The main goal of the preprocessing step is usually to reduce noise in input images but can also be used to increase the contrast of bright structures such as exudates. In color fundus photographs different bright structures are present such as the optic disc, which appears as a large, bright disc and is present in each image but also some structures such as drusen and optic nerve fibers, which do not appear in each image. Such bright structures can decrease the performance of exudate detection algorithms so one of the main goals of image preprocessing is to detect and remove such bright structures from original images. In Fig. 6.1 we can see several bright structures such as drusen marked with arrow *b* and optic nerve fibers marked with arrow *a*, which come out of the optic disc and are usually visible near the main vessels. The optic disc is marked with a black circle.

In the literature we can find different preprocessing methods used in algorithms for detection of anatomic structures in retinal images of which many are presented in [81]. For example, authors use histogram equalization, adaptive histogram equalization, division by over-smoothed version of the original image in order to increase contrast levels, where the original intensity

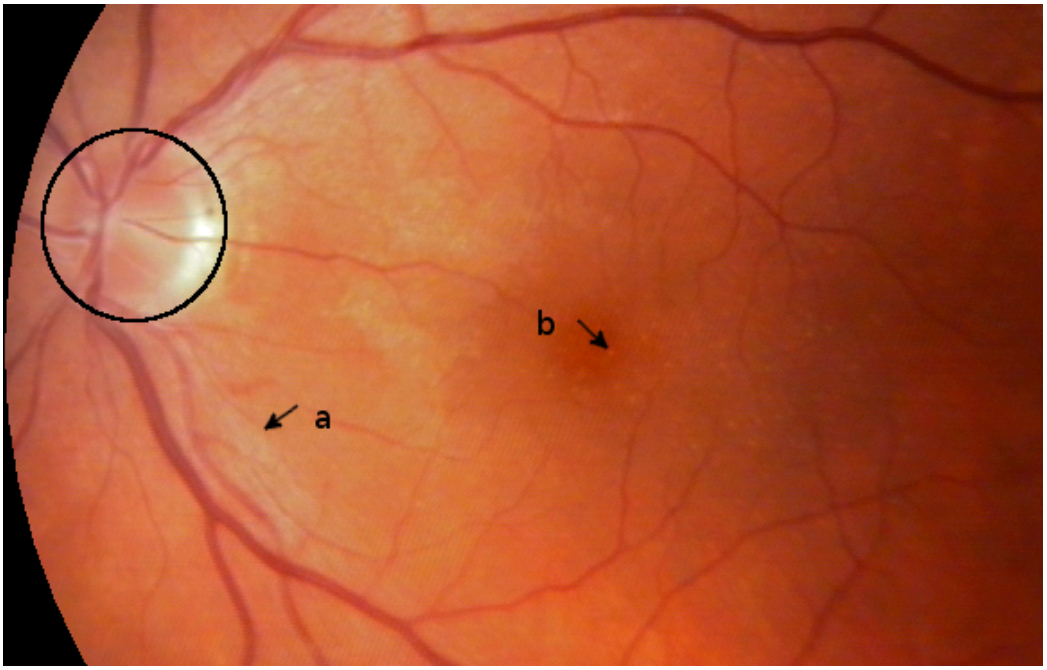

Fig. 6.1: Bright structures in healthy patients: a) Optic nerve fibers and b) drusen

image is normalized by dividing the original intensity image by an over-smoothed version of the original image using a spatially large median filter [82], Gray World normalization [83] where normalization is performed by dividing each color channel by its average value, illumination equalization where pixel values are modified by subtracting the mean intensity value calculated in a window.

After preprocessing, a candidate extraction procedure is applied in order to detect potential exudate areas. In the literature, we can find many different approaches for candidate extraction such as methods based on morphological operations [50, 84, 85, 86], dynamic thresholding approaches [87], pixel-wise feature extraction and classification [26, 85, 88, 89], clustering based approaches [90]. For example, in [84] authors start the exudate detection procedure by finding areas with high standard deviation in a sliding window followed by a thresholding procedure. In order to find the precise border of each exudate area, morphological reconstruction by dilation is used where the generated binary image is used for morphological reconstruction. The reconstructed image is then subtracted from the original image and after a final threshoding procedure a binary image containing exudate pixels is generated. In [87] authors used a Gaussian mixture model for histogram modelling. They used the Expectation Maximization algorithm to estimate the mixture parameters for the Gaussian distributions. After parameter estimation, a dynamic threshold based on two Gaussian components with highest mixing weights is found and applied in order to segment the image into exudate and non-exudate regions. In [26, 85] authors used pixel-wise features such as difference of Gaussians, standard deviation in a window, hue, saturation, mean intensity values, maximum values, difference between highest and lowest value in a window, entropy, edge strength and then apply different classifiers such as K-Nearest Neig-

hbours or Naive Bayes in order to classify each pixel as as an exudate or non-exudate. In [90] authors applied the Fuzzy C-Means clustering algorithm on locally contrast enhanced image. In this approach RGB values for each pixel were used as input features for the clustering algorithm. After clustering, elements in the brightest cluster we assigned as exudate pixels. In [91] authors use the k-means clustering procedure on raw image pixels but also add output of the Kirsch edge operator as clustering features in order to remove areas with low edge strength.

After candidate extraction different features can be extracted for each connected component in order to eliminate spurious regions. Features such as area, length, perimeter, ratio of major and minor axis, average value inside the exudate area, mean and standard deviation of Gaussian derivative filter outputs in the candidate area are extracted from each exudate candidate [92, 93]. Some of the authors proposed features, which take into account the environment of the exudate candidate, for example distance from the blood vessel because exudates typically do not appear near the main vessels [94].

6.1 Weighted ensemble based exudate detection

Accuracy of existing exudate detection algorithms can be improved by combining different exudate detection algorithms into an ensemble because s many of the proposed algorithms have some drawbacks but by combining the outputs of different algorithms we can expect better results. We start by applying different candidate extraction algorithms for each image. This generates large number of potential exudate candidates. For each exudate candidate extracted by the ensemble we calculate different morphological and statistical features, which are used for classification of each potential exudate candidate. In Fig. 6.2 we can see the flowchart of the proposed ensemble method.

In the following subsections we describe which preprocessing methods and candidate extraction methods are used, how they are combined into an ensemble and finally how the machine learning based classification is performed.

6.1.1 Preprocessing methods

In order to increase the candidate extraction algorithms performance we can apply different preprocessing algorithms. In this subsection we present different preprocessing methods used in creation of the ensemble.

- Green Channel Extraction: Green channel is the channel with the highest contrast between the background and other important parts like lesions, so using only the green channel can improve the accuracy of an exudate detection algorithm.
- CLAHE: Contrast-Limited Adaptive Histogram Equalization (CLAHE) is a well-known

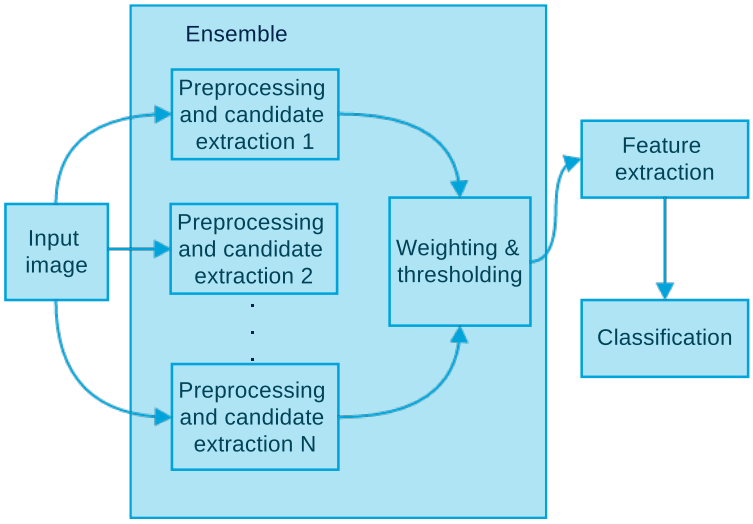

Fig. 6.2: Flowchart of the proposed weighted ensemble based exudate detection method.

contrast enhancement technique, which is used because some exudate detection algorithms rely on good contrast between exudates and the background. This preprocessing algorithm is very similar to the adaptive histogram equalization method but also adds histogram clipping at a predefined value before computing the cumulative distribution.

- Gray-World Normalization: Gray-World Normalization is used as a preprocessing method because it can eliminate effects due to illumination changes, so it is used to eliminate the shining along temporal arcades. Gray World normalization performs the normalization by dividing each color channel by its average value.
- Illumination correction: The illumination of the input image is non-uniform, which is caused by spherical shape of the eye and different tissues present in the eye. In order to compensate this type of non-uniformity a median filtered image is subtracted from the original image where the median filtering is performed using a large mask in order to properly estimate the median value of the region.
- White Top-Hat Transformation: This simple morphological transformation is used for highlighting brighter regions and because exudates appear as bright, yellowish structures this transformation can be used to increase the contrast of exudate regions. In order to perform the white top-hat transformation the result of grayscale opened image is subtracted from the original image. Grayscale opening is performed by first performing grayscale morphological erosion followed by grayscale morphological dilation.
- Contrast enhancement (Contrast): This method was proposed in [95] and starts by converting the original RGB image to YIQ color space. In this color space the original Y channel is replaced by a weighted sum of the channels Y, I and Q according to (6.1).

$$Y_{mod}(x,y) = 1.5 \cdot Y(x,y) + (-1) \cdot I(x,y) + (-1) \cdot Q(x,y) \tag{6.1}$$

Apply applying the correction, the modified image is converted back to the RGB color space. In the new image, bright regions are amplified so they appear brighter and dark regions become darker.

- Adaptive contrast enhancement: In this preprocessing method the contrast of the input images is improved by changing the illumination of the original image using (6.2)

$$I_{eq}(x,y) = (I(x,y) - I_w(x,y))/\sigma_w(x,y) \tag{6.2}$$

where $I(x,y)$ is the original intensity image, $I_w(x,y)$ is the mean intensity value within a local neighborhood of point (x,y) and $\sigma_w(x,y)$ is the standard deviation of intensity within a local neighborhood of point (x,y). Areas with low contrast typically have a smaller standard deviation of intensity in their neighborhood so dividing the difference between original and background image with the standard deviation increases contrast more in areas with low contrast.

6.1.2 Candidate extraction algorithms

After image preprocessing a candidate extraction step is performed in which potential exudate regions are coarsely found. In this subsection we present the candidate extraction algorithms used for the ensemble creation.

Morphological-based candidate extraction algorithm

The morphological-based candidate extraction algorithm uses the approach presented in [84] where authors proposed a method for detection of exudates using morphological operations. Because of usually high contrast between exudate regions and surrounding background the method assumes that exudate regions are regions with large standard deviation. In order to detect the exudates, the method starts with morphological closing, which is actually morphological dilation followed by morphological erosion of the input image with a large structuring element. This step is performed in order to eliminate the blood vessels, which also show large local deviation due to contrast of blood vessels compared to the surrounding background. After this step, the standard deviation in a sliding window is calculated and a fixed threshold is applied to find the candidate regions with high standard deviation. The candidate regions are dilated to ensure that the background pixels next to exudates are included in the candidate regions. In order to find the contours of the exudates and to distinguish them from other well contrasted regions all the candidate regions are set to zero in the original image and then morphological reconstruction by dilation of the original unchanged image under the new image is performed. With this procedure exudates are completely removed from the image. The final result is obtained by applying a simple threshold operation to the difference between the original image

and the reconstructed image. In this way only the candidates that have a contrast level above a minimum threshold level are selected as exudate regions.

Local and global thresholding-based candidate extraction algorithm

The thresholding candidate extraction algorithm is based on work by [96] where the authors segment the bright regions in the preprocessed image that show high global and local brightness levels. This method assumes that exudates are locally and globally bright regions. The method starts by calculating a global histogram and several local histograms by partitioning the original image into non-overlapping square blocks. The blocks have to be large enough to ensure that enough background pixels are present in each block, which allows the local differentiation of background from bright regions but small enough to capture the local properties of the image. Global and local histograms are usually bell shaped and they show one maximum corresponding to the background and one tail on each side of the maximum. To separate the bright regions from the background a threshold is set at the gray level of the right tail of the histogram for which the histogram decreases to a 10% of the histogram maximum. As a result of the histogram thresholding process two binary images are obtained. One binary image contains regions which are globally bright and the other image contains regions, which are locally bight. In order to find the final binary image containing locally and globally bright regions two images are combined using the logical AND operation.

SVM-based candidate extraction algorithm

In this approach, various features for each pixel are extracted and a linear SVM classifier is used to decide if the pixel belongs to an exudate region or if the pixel belongs to the background. The features are selected from a range of various features, which are relevant for exudates such as the mean, standard deviation, maximum value, range (difference of maximum and minimum) of the intensities within a window. RGB value of the pixel being classified is also added to the feature vector. In the literature [26] it has been shown that Gaussian derivative taken at different scales can be used for pixel-wise detection of exudate so responses to zero, first and second order Gaussian derivatives are added to the feature vector. Because exudate regions are usually regions with sharp edges the Frei-Chen edge detector is applied to the original image and different features such as the highest gradient value, average and standard deviation of the strength of the edge pixels and number of the edge pixels in the pixel neighborhood are added as the features of the feature vector. Output of the classifier is a binary image with exudate candidates marked with the label “one” and background pixels marked with the label “zero”. In order to train the SVM classifier per pixel label image of exudate regions is required. We use the DRiDB [97] database, which is explained in more detail in **??** for classifier training.

Clustering-based candidate extraction algorithm

The clustering-based candidate extraction algorithm uses the approach described in [91] where the authors used a k-means based clustering procedure to find exudate regions. The procedure starts by using raw image pixels as feature vectors for k-means clustering. After applying k-means clustering and taking the cluster with the highest mean value some structures, such as the papillary region and other yellow lesions, such as cotton wool spots are detected, because of their similar attributes to hard exudates in terms of brightness, color and contrast. In order to detect only hard exudates characterized by yellowish color and sharp edges and remove all lesions with high intensity but blurred edges such as cotton wool spots an edge strength criterion is used. In order to measure the edge strength Kirsch operator [98] is applied to the original image and the resulting image is thresholded using a fixed threshold. In order to remove spurious regions a boolean AND operation between the original k-means clustered image and the thresholded edge image is performed. This operation finds only the edges of bright objects. Finally, in order to find the exudate regions morphological reconstruction by dilation under the retinal image of the green channel from the original image is performed.

6.1.3 Combining candidate extraction algorithms

Combining different preprocessing and candidate extraction algorithms into an ensemble can increase the accuracy of exudate candidate detection. In the proposed approach we start by creating a pool of possible pairs of preprocessing methods and candidate extraction methods explained previously. In the case of a <preprocessing method, candidate extraction method> pair, the given preprocessing method is applied before performing the given candidate extraction method. The simulated annealing search algorithm [59] is used to find the optimal weights for each of the <preprocessing method, candidate extraction method> pairs present in the ensemble. The simulated annealing search algorithm is used because this problem represents a non-linear optimization problem. In order to evaluate the goodness of the solution energy function given by (6.3) is used.

$$E = -F_{score} = -\frac{5 \cdot \text{sensitivity} \cdot \text{PPV}}{4 \cdot \text{PPV+sensitivity}} \tag{6.3}$$

In the equation (6.3), sensitivity is defined as $TP/(TP+FN)$ and positive predictive value (PPV) as $TP/(TP+FP)$, where TP is the number of true positive pixels, FN is the number of false negative pixel and FP is the number of false positive pixels. A pixel is classified as a true positive if the pixel is marked as an exudate pixel in both the ground truth image and in the binary image created using current weights. A pixel is classified as a false positive if the pixel is marked as an exudate pixel in the binary image created using current weights but not in the ground truth image. A pixel is classified as a false negative if the pixel is marked as an exudate pixel in the ground truth image but nut in the binary image created using current weights. When

the simulated annealing algorithm picks the weights a weighted image of the binary images produces by each <preprocessing method, candidate extraction method> pair is created. The weighed image is then normalized to [0,1] interval by dividing each image element with the sum of weights, which are used for creation of the weighted image. In order to evaluate the energy function the weighted image has to be thresholded. Because the image is normalized to [0-1] range the pixel values in this image can be treated as probabilities of pixels being part of an exudate region. In order to create a thresholded image a fixed threshold of 0.5 is used.

The energy function used is actually the F_2 score measure. This measure was chosen in order to increase the effect of sensitivity in the energy function. This is used because in the subsequent exudate classification step a lot of false positive exudate candidates can be eliminated but no new exudate regions can be added. Eliminating false positive regions in the exudate classification step will lead to higher positive predictive value and finally to higher overall accuracy of the algorithm.

6.1.4 Exudate classification

After finding the optimal ensemble weights the ensemble can be used to extract potential exudate regions in unseen images. After finding the potential exudate regions different features for each exudate candidate regions can be extracted. To find efficient features for classification, several shape and statistical descriptors for exudate candidates are calculated and the most useful ones are selected by using a Wilcoxon rank test[99]. Most obvious features that can be extracted and are used in the literature are the mean, standard deviation, difference between maximal and minimal value, minimal and maximal values under the given region and under the boundary of the region using the intensity values of the image. Also, the mean, standard deviation, difference between maximal and minimal value, maximal and minimal values of the intensities under the region and under the boundary of the region in the green channel, CLAHE image, illumination corrected image are added to the feature pool. Because first and second order Gaussian derivatives have shown good discriminative power the mean and standard deviation of zero, first and second order Gaussian derivatives taken at different scales are calculated under the region and added to the feature pool. Homogeneity of the the region measured in terms of the Shannon's entropy of the RGB values calculated for each channel is added to feature pool. Several morphological features like exudate candidate area, major and minor axis length and compactness are also added to the feature pool.

During experimentation it was noticed that a lot of false positive exudate areas are visible near the main arteries and veins, especially in younger patients so it was decided to add distance from main veins and arteries as a feature to the feature pool. Since exudates often appear close to the center of the image distance from the optic disk was added as a feature to the feature pool.

Most of the mentioned descriptors are appropriate for distinguishing between exudate and

non-exudate regions. However, there are some irrelevant descriptors and these can decrease the generalization performance of the trained classifier. To select the most significant descriptors the Wilcoxon rank test was used as mentioned.

After selecting the best features the AdaBoost classifier was used for exudate classification. A small subset of feature vectors was used for training and all other feature vectors were used for testing purposes.

6.2 Performance evaluation

The testing was done on the DRiDB database [97], which is presented in more detail in Chapter 3. The database was split into two disjoint sets for training and testing purposes.

To test the method the ground truth data available in the mentioned datasets was used. For each image, number of true positives (TP), false positives (FP) and false negatives (FN) is calculated. Measuring the true positives, false positives and false negative could be done by counting the number of pixels, which are correctly classified but this approach has some drawbacks because it can happen that we actually detect the exudate blob correctly but because the ground truth segmentation is not perfect several border pixels can be assigned as false positive or false negative. In order to solve this problem the approach explained in [100] was used. Each segmented image can be divided into a set of candidates $\{C_1, C_2, \ldots, C_N\}$ where each C_i represents a connected component. Each ground truth image can also be divided int a set of candidates $\{G_1, G_2, \ldots, G_M\}$. So the ground truth mask is given by (6.4).

$$G = \bigcup_{1 \leq j \leq M} G_j \tag{6.4}$$

The segmented images can be represented with (6.5).

$$C = \bigcup_{1 \leq i \leq N} C_i \tag{6.5}$$

A pixel is considered to be a true positive pixel if, and only if, it belongs to any of the following sets:

- $C \cap G$
- C_i such that $\frac{|C_i \cap G|}{|C_i|} > \sigma$
- G_j such that $\frac{|G_j \cap C}{G_j} > \sigma$

Here, $|,|$ represents number of elements in set and σ is a parameter in $[0,1]$ range. A pixel is considered to be a false positive pixel if, and only if, it belongs to any of the following sets:

- C_i such that $C_i \cap G = \emptyset$
- $C_i \cap \bar{G} \leq \sigma$

A pixel is considered to be a false negative if, and only if, it belongs to any of the following sets:

- G_j such that $G_j \cap C = \emptyset$
- $G_j \cap \bar{C}$ such that $\frac{|G_j \cap C|}{|G_j|} \leq \sigma$

The true negatives are omitted from the analysis because the number of true negatives can be very high since all non exudate pixels are actually true negatives. The σ was set to 0.2.

The sensitivity S of detection is calculated using (6.6),

$$S = \frac{TP}{TP + FN} \tag{6.6}$$

and the positive predictive value (PPV) using (6.7).

$$PPV = \frac{TP}{TP + FP} \tag{6.7}$$

Finally the F-score is calculated using (6.8)

$$F = \frac{2 \cdot S \cdot PPV}{PPV + S} \tag{6.8}$$

Table 6.1 presents the results of the experimental validation after 3-fold cross-validation for the DRiDB database. The proposed method outperforms all algorithms used in the validation process. From the table it can be seen that the method shows good balance between sensitivity of detection and positive predictive value of detection, which is consistent with the optimization function used during the training process.

Table 6.1: Results of different exudate detection methods.

Method name	Sensitivity	PPV	F-Score
Walter [84]	0.69	0.48	0.57
Sánchez [95]	0.34	0.61	0.44
Harangi [85]	0.66	0.65	0.66
Harangi [93]	0.71	0.66	0.68
Amel [91]	0.41	0.09	0.15
Weighted ensemble based exudate detection method	0.75	0.77	0.76

In Fig. 6.3, we can compare the ground truth marked by an expert with the output obtained by the weighted ensemble based exudate detection method. It can be clearly seen that the results are pretty good and most of the candidates are properly detected. The method fails in detecting small isolated exudate areas, which are similar to other normal structures in eye fundus. Sometimes, nearby regions are merged into one larger exudate cluster, which causes

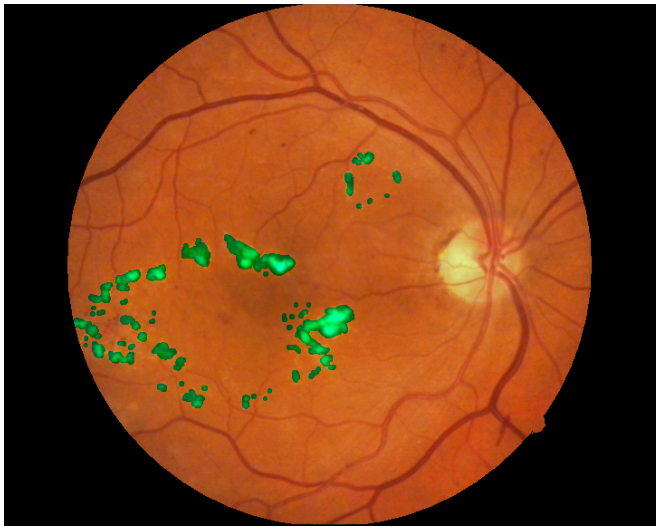

(a) Ground truth data

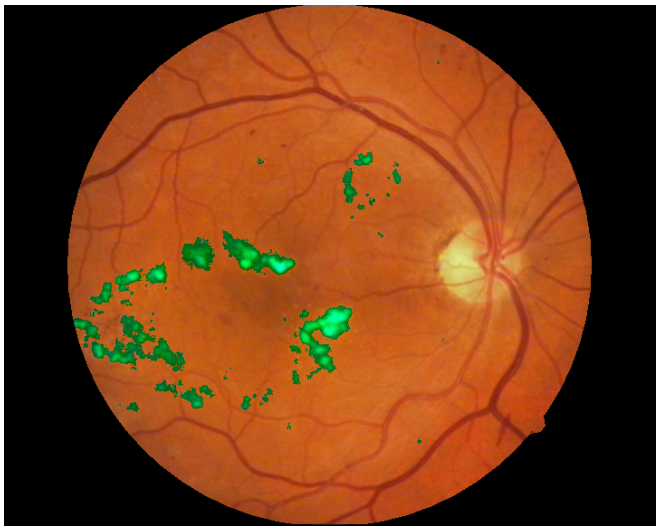

(b) Output of the weighted ensemble method

Fig. 6.3: Comparison of ground truth with output of the weighted ensemble method.

some false positive detections but this is expected.

Chapter 7

Automatic early detection of diabetic retinopathy using rule-based system and specific ophthalmologic knowledge

In order to improve the overall performance of a system for early detection of diabetic retinopathy information obtained by detecting normal structures can be combined with detection results of patholological structures. In this chapter we present a method for automatic early detection of diabetic retinopathy using a rule based system and specific ophthalmologic knowledge about normal and pathological retinal anatomy

In the proposed method outputs of different anatomical landmark detection algorithms are combined with a deep learning based exudate detection procedure in order to increase the overall accuracy of exudate detection, which is a prerequisite in development of a system for early detection of diabetic retinopathy. The general flowchart of the method explained in following paragraphs is visible in Fig. 7.1.

According to the flowchart we can see that the information about blood vessel locations, bright borders and optic disc location is used to increase the exudate detection performance. The exudate detection is done using a deep convolutional neural network, which is applied to the preprocessed image.

The optic disc detection is performed by combining outputs of different simple optic detection algorithms, which generate optic disc probability maps. In this map, higher values represent increased probability that this point belongs to the optic disc. The procedure is explained in more detail in Chapter 4.

Parabola fitting is performed using information about the optic disc center and information about the main blood vessels. The output of this step is a probability map, with higher values representing regions with higher probability of containing exudates. This procedure is explained in more detail in Sec. 7.2.

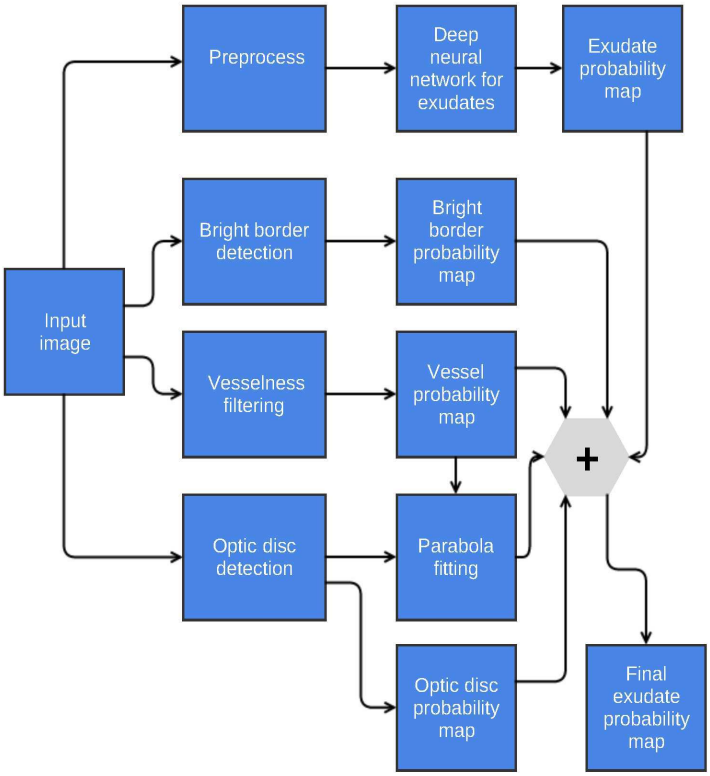

Fig. 7.1: Flowchart of the proposed fusion based method for exudate detection. Outputs of vessel detection and optic disc detection methods are combined with the output of the deep neural network in order to increase the accuracy of exudate detection.

Probability maps related to blood vessels, optic disc, parabola fitting and values for the bright border detection are combined together to get one probability map. This map is created using a simple weighted sum of per pixel probability maps, were weights were found empirically. This map incorporates higher level ophthalmolgical knowledge about diabetic retinopahy. Example of such information is that exudates do not appear inside of the optic disc or inside blood vessels. The contrast and brightness of the optic disc can affect the performance of the exudate detection procedure so it is a common practice to eliminate the optic disc area before applying the exudate detection algorithm. In our case, removal of the optic disc is performed by assigning zero probability of exudate appearance inside of the optic disc. Also, exudates have lower probability of appearing near the main blood vessels. This information can be used to define regions with small probability of containing exudates. In order to dynamically define such regions it is necessary to detect the blood vessels and find the optic disc and then use this information to define regions with low exudate probability. Because bright structures such as

optic fibers appear near the main blood vessels assigning lower probability of exudate appearance in those areas can decrease the number of false positive detections and lead to higher overall accuracy of exudate detection. Due to imaging artefacts some fundus images contain extremely bright regions along the border of the fundus image. Detecting such areas and assigning lower probabilities of exudate appearance in those areas can decrease the number of false positive detections and increase the accuracy of the exudate detection procedure.

7.1 Detection of bright borders

Some images have extremely bright regions along the border of the visible part of the fundus image. Those regions can cause problems with exudate detection because they are very bright. Example of such a border is marked in Fig. 7.2. In order to account for such anomalies the

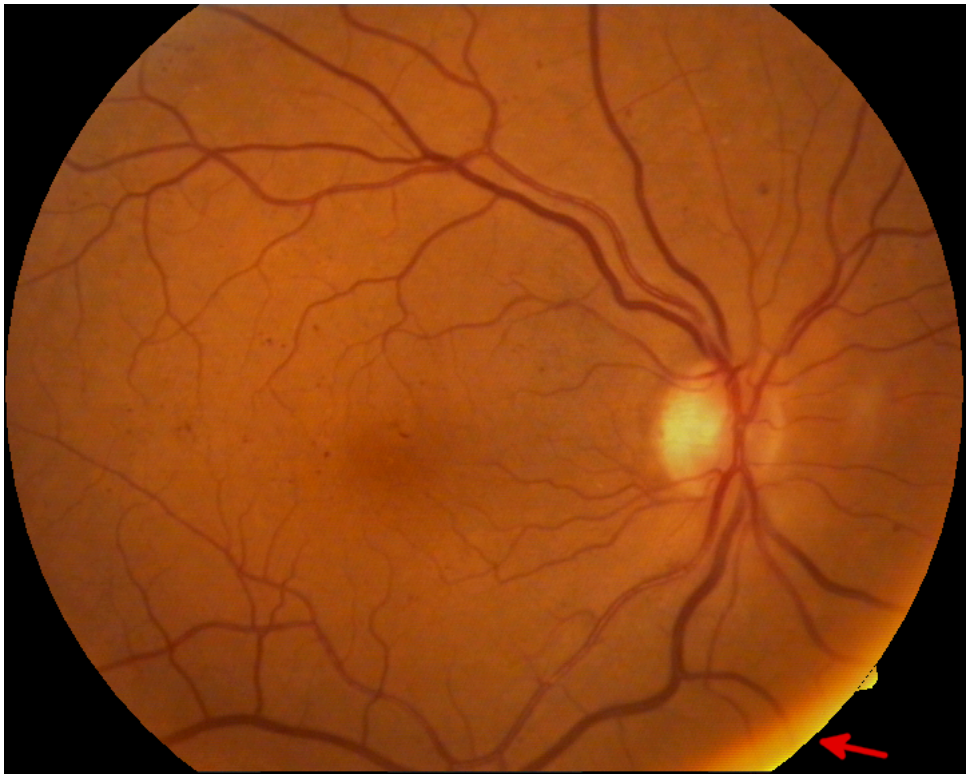

Fig. 7.2: Image with bright border marked

bright border should be segmented if it is present in the image. Using this information areas with low exudate probabilities can be defined because exudates should not appear inside of those areas. This probability map is then incorporated in the exudate detection procedure.

The approach explained here builds upon the method presented in [100] so the green channel of the original image is taken and a large median filter is applied to the green channel in order to estimate the background of the image. After that the estimated background is subtracted from the green channel in order to remove the background from the image. Only positive values are

kept and negative values are set to zero. This eliminates structures darker than the background. Because we are only interested in bright areas around edges of the field of view the bright regions inside of the retina need to be eliminated. This is done by creating an attenuation map for each pixel of the image. Values of the proposed map are calculated using (7.1) where $S(x,y)$ is the value of the attenuation at point (x,y), $D(x,y)$ is the distance from the closest point to the edge of the field of view and a is a positive constant. In our experiments, a was set to 0.02.

The field of view mask can be easily calculated using a simple thresholding procedure. Image pixels outside of the field of view are zero or close to zero so applying a low threshold will segment the field of view. The field of view mask in this case is just the largest blob in the obtained binary image. In order to fill any potential holes in the field of view mask a filling operation is performed.

$$S(x,y) = \exp^{-a \cdot D(x,Y)} \tag{7.1}$$

Fig. 7.3: Bright border segmented

The attenuation map is then applied to the green channel with the estimated background subtracted. This creates a new image in which only bright regions near the edge of the field of view are preserved. In order to eliminate darker pixels a fixed threshold to this new image is applied. Pixels with values less than the threshold are set to zero and all other pixels are left unchanged. The threshold was empirically found. In this new image, higher values represent bright points near the border. Example of such an image can be seen in Fig. 7.3.

7.2 Parabola fitting

Most reflections and optic fibers are found along the main retina vessels and they lie inside a parabolic region passing through the optic disc. In order to eliminate the false positive exudate regions caused by such bright structures a symmetric double parabolic region passing through the optic disc center is fitted. The parabola is fitted to the largest blood vessels, which converge around the optic disc area, which is similar to the approach presented in [101]. In Fig. 7.4 we can see a parabolic region drawn on top of the original image.

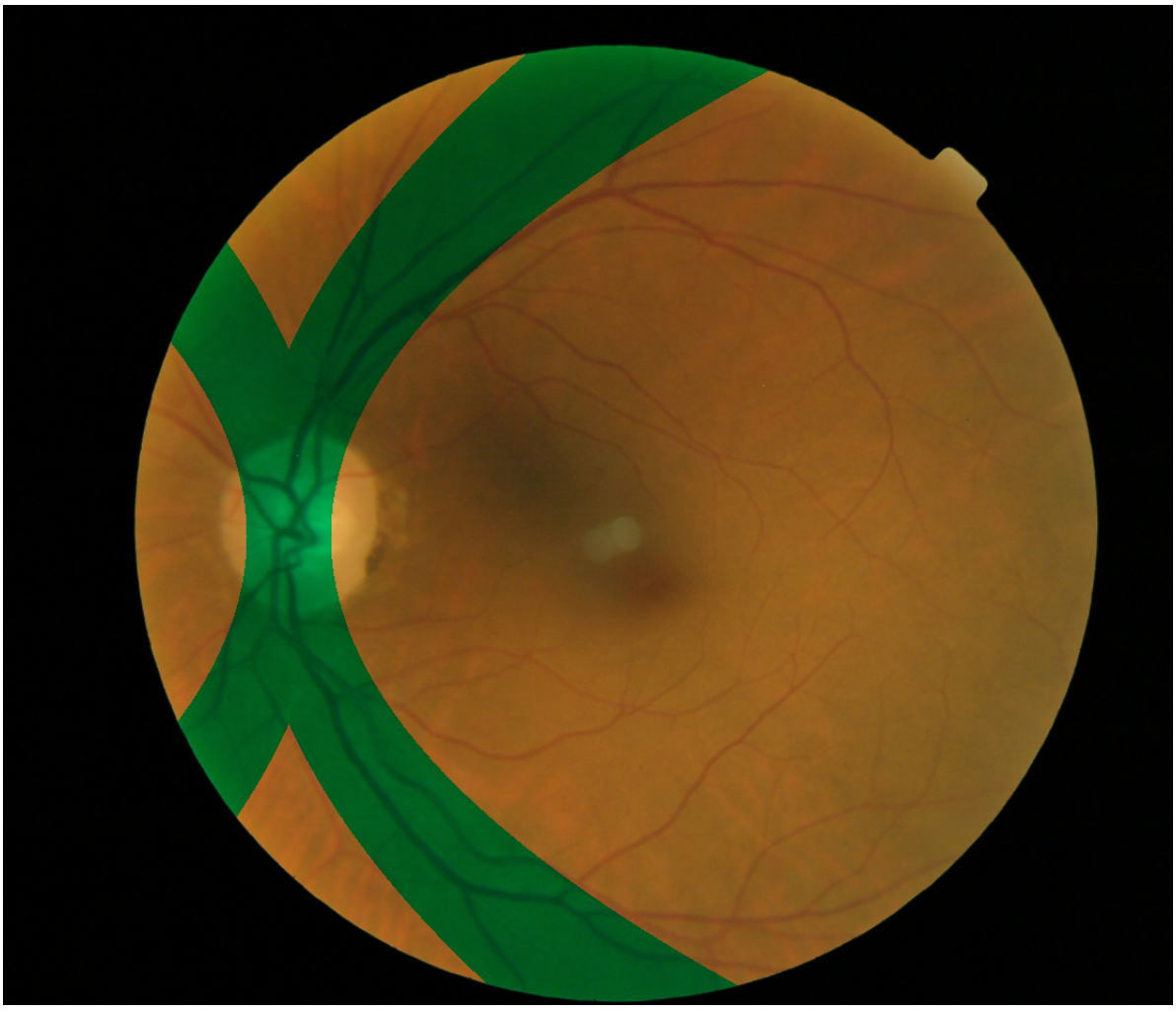

Fig. 7.4: Parabola fitted to main vessels

In order to perform parabola fitting the location of the optic disc is required and blood vessels should be segmented. In order to segment main blood vessels we start with the blood vessel image and take 10% of the thickest blood vessels. This is done by iteratively eroding the binary vessel image. After this step the blood vessels are thinned so all blood vessels are only one pixel thin. The remaining points after thinning are the points used to estimate the parabola. Because the parabola should be shifted to the optic disc center (x_{OD}, y_{OD}) the resulting parabola

equation is given by (7.2).

$$a \cdot (y - y_{OD})^2 = |x - x_{OD}| \tag{7.2}$$

The only unknown parameter is the scaling factor a. This parameter is found by applying the standard non-linear Marquardt [80] optimization procedure to the criterion function J from (7.3) where S is the set of points in blood vessel image after thinning. The optimization procedure converges quickly, usually in less than 10 iterations.

$$J(a) = \sum_{(x,y)\in S} a \cdot (y - y_{OD})^2 - |x - x_{OD}| \tag{7.3}$$

The main purpose of parabola fitting is to define regions with low exudate probability. The regions around main blood vessels tend to contain many reflections and optic fibers, which can decrease the performance of the exudate detection algorithm. In our case an adaptive probability mask for those regions based on parabola fitting of main vessels is created. So regions, which are close to the parabola should have low probability of exudate appearance, and regions far away should have higher probability of exudate appearance. This is modeled by using a distance function from the fitted parabola. The probability of exudate appearance is defined by the distance function in(7.4).

$$P(x,y) = 1 - \exp^{-a \cdot D(x,y)} \tag{7.4}$$

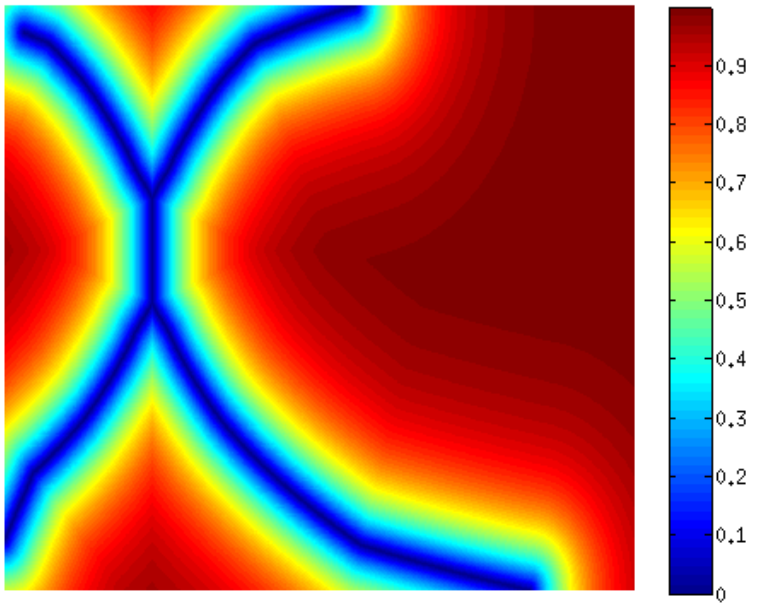

Fig. 7.5: A priori exudate probability map generated from parabola fitting procedure

Here, $P(x,y)$ is the a priori probability of point (x,y) containing exudates, $D(x,y)$ is the euclidean distance of point (x,y) from the parabola fitted to the main vessels and a is a small positive constant. Example of the proposed a priori probability function can be seen in Fig. 7.5. Blue values mean that there is a small probability of finding exudates in that area and red

that there is a high probability of finding exudates in that area. This probability map is later combined with output of the exudate detection procedure to increase the accuracy of exudate detection.

The exponential function was chosen as the generator function for the a priori probability map because the exponential function has only one tunable parameter (small positive constant a), which was empirically found.

7.3 Convolutional neural network for exudate detection

In order to detect exudates semantic information from optic disc detection, bright border detection, parabola fitting, blood vessel detection is combined with the output of the convolutional neural network. In convolutional neural networks used as semantic segmentation tool feature extraction is learned from the data and not enforced by designers. Approaches based on convolutional neural networks obtained state of the art results in a very broad range of applications [102]. The exudate detection procedure starts with a preprocessing step.

7.3.1 Preprocessing

In order to reduce the noise levels in fundus photographs before using the convolutional neural networks for exudate detection the Total Varaiation (TV) regularization denoising is used, which was originally developed for additive white Gaussian noise denoising by Rudin, Osher and Fatemi [103]. The authors proposed to estimate the denoised image u as the solution to the minimization problem in (7.5),

$$\underset{u\in BV(\Omega)}{\arg\min}\,||u||_{TV(\Omega)} + \frac{\lambda}{2}\int_{\Omega}(f(x)-u(x))^2\,\dot{\mathrm{x}} \tag{7.5}$$

where λ is a positive parameter. Here, f is the observed noisy image, which is related to the underlying true image u by $f = u + \eta$, and η is at each point in space independently and identically distributed as a zero-mean Gaussian random variable. This problem is referred to as the Rudin-Osher-Fatemi or ROF problem.

In our case total variation is the integral of its gradient magnitude given by (7.6).

$$||u||_{TV(\Omega)} = \int_{\Omega}|\nabla u|\,\dot{\mathrm{x}} \tag{7.6}$$

Such formulation of the minimization function discourages the solution from having oscillations, yet it does allow the solution to have discontinuities. This is possible because if u is monotonic in $[a,b]$ then $TV(u) = |u(b)-u(a)|$, regardless of whether u is discontinuous or not.

The second term in (7.5) encourages the solution to be close to the observed image f. By this combination, the minimization finds the denoised image.

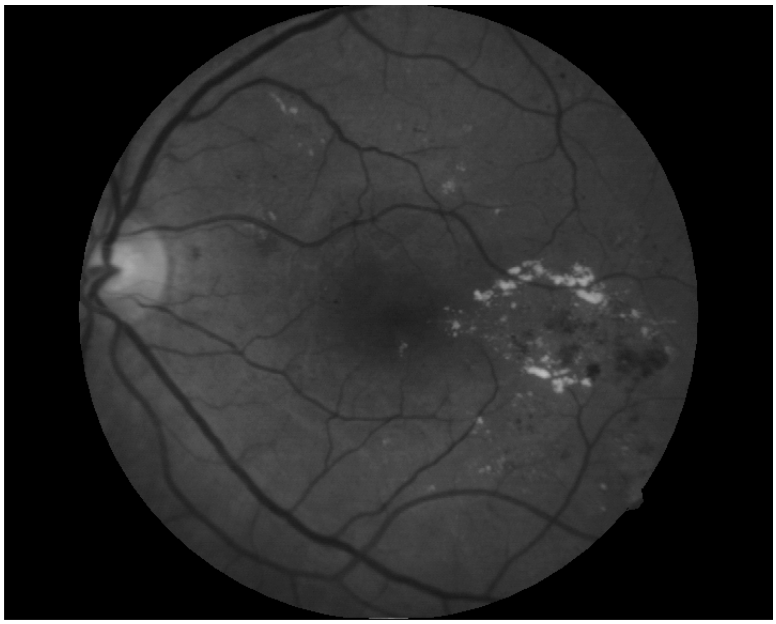

Fig. 7.6: Original noisy image

In order to perform the denosing the split Bregman algorithm is used, which is explained in more detail in [104, 105].

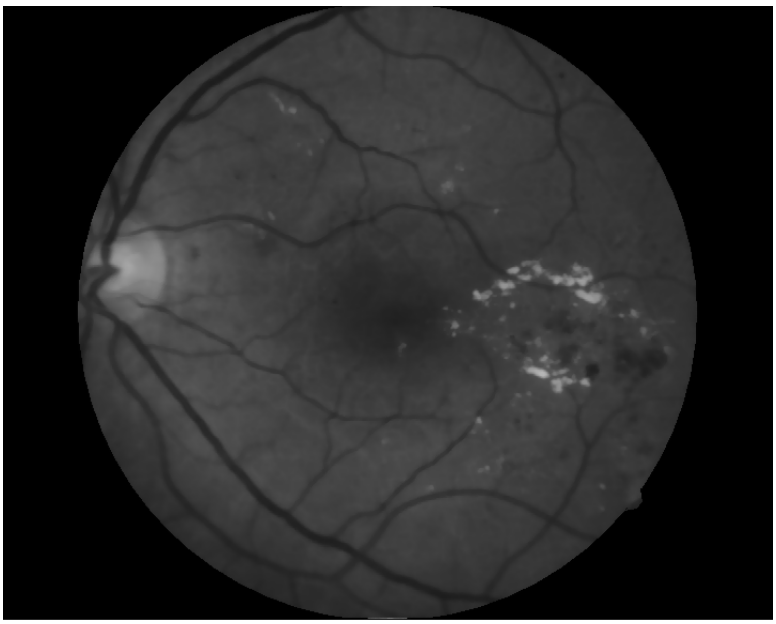

Fig. 7.7: Denoised image

In Fig. 7.6 it can be seen how the original image looks like, and in Fig. 7.7 it can be seen how the denoised image looks like. Small section of the original and denoised image is shown in Fig. 7.8. Obviously, it can be seen that noise levels are reduced and all edges are still present. This is important because hard edges are one of the main characteristics of exudates.

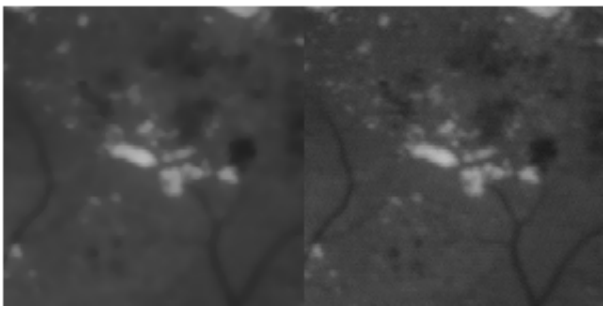

Fig. 7.8: Denoised image (left) and noisy image (right)

7.3.2 Convolutional neural network architecture

After preprocessing, a deep neural network is applied. For exudate detection the convolutional neural network (CNN) is used, which is a specific type of a deep learning structure. Our method is inspired by work presented in [106] where authors used deep neural networks in order to segment neuronal membranes in electron microscopy. The classification goal of our convolutional neural netowork is to classify each pixel in *exudate* or *non-exudate* class. Our convolutional neural network calculates the probability of a pixel being one of the mentioned two classes. Inputs of the network are raw intensity values in the total variation preprocessed image of a square window centered in the pixel p, which is currently processed. The size of the window is an odd number in order to enforce symmetry around the given pixel. For pixels near the image border, the window would include pixels outside the image boundaries. In those cases new values in the sliding window are inserted by mirroring the pixels from window which fall inside the image.

The convolutional neural network is first trained using images from the training set. After training, in order to segment the image, the convolutional neural network has to be applied for each image pixel. This means that output of the image classification is another image where each pixel value represents the probability of the pixel being an exudate. In order to get a binary image a fixed threshold would have to be applied. In our case the probability maps for blood vessels, optic disc, parabola fitting and bright border as a priori information are combined with the output of the convolutional neural network in order to create the final exudate probability map. This map can then easily be thresholded in order to get the exudate areas.

A typical convolutional neural network consists of a sequence of convolutional, max-pooling and fully connected layers [106]. This type of deep neural network is hierarchical feature extractor, which uses raw pixel intensities of the original image in order to create a new feature vector, which is then classified by several fully connected layers. This is the main difference compared to other machine learning approaches where we have to manually decide on the features to be used in a classifier because, in the convolutional neural networks the filters are automatically learned from training data. Each convolutional layer from the network performs a 2D convolution of its input images called input maps with a sequence of square filters. Output

of each input map is calculated by summing the convolutional responses over the whole input map. After that, this sum is passed through a non-linear activation function. Finally, a max-pooling layer downsamples the output of non-linear activation function by a constant factor. Their outputs are given by the maximum activation over non-overlapping square regions. Max-pooling layers are fixed, non-trainable layers, which select the most promising features [107]. After a few stages of alternating convolutional and max-pooling layers outputs of the final max-pooling layer are brought as inputs to a sequence of fully connected layers. The output layer is a fully connected layer with one neuron per class, which in this case equals to two neurons. A softmax activation function after the last layer was added so the output of the convolutional neural network can be treated as the probability of a particular image pixel belonging to the exudate class. The architecture of the convolutional neural network is visible in Table 7.1. It can be seen that there are four convolutional layers and four max-pooling layers. The size of the input map is 65×65, which means that in order to classify a pixel, convolution in a window of size 65×65 is performed in the input layer. As it was mentioned, before max-pooling a non-liner activation function is applied. In this proposed architecture a rectifying linear unit is used as the non-linear activation function.

Table 7.1: Architecture of used convolutional neural network

Layer	Type	Maps and size	Kernel size
0	input	1 map of 65×65 neurons	-
1	convolutional	48 maps of 60×60 neurons	6×6
2	max pooling	48 maps of 30×30 neurons	2×2
3	convolutional	48 maps of 26×26 neurons	5×5
4	max pooling	48 maps of 13×13 neurons	2×2
5	convolutional	48 map of 10×10 neurons	4×4
6	max pooling	48 maps of 5×5 neurons	2×2
7	convolutional	48 maps of 4×4 neurons	2×2
8	max pooling	48 maps of 2×2 neurons	2×2
9	fully connected	100 neurons	-
10	fully connected	2 neurons	-

To train our convolutional neural network, we use all available positive training samples from our training images. From each image, we take all the exudate pixels as positive samples and the same amount of pixels randomly sampled among all non-exudate pixels but without repetition. We perform this in order to have a balanced training set. Because exudates can appear in different shapes and orientations andi in order to augment the training set we synthetically add rotated and mirrored versions of training samples. Positive and negative sample are interle-

aved so to have approximately equal number of positive and negative samples when randomly sampling the training set. We take the green channel as the input to our network because it contains the most contrast according to the literature [108].

Initial convolutional kernel weights were drawn from a Gaussian distribution with zero mean and standard deviation of 0.01 and initial weights of fully connected layers were drawn from a Gaussian distribution with zero mean and standard deviation of 0.1. Batch size during the training phase was set to 100 and the network was trained for 200 000 iterations. The training was stopped when there was no significant improvement of accuracy on the validation set.

7.4 Performance evaluation

Training and testing of the proposed deep learning method was done using a computer with a Tesla K20C graphics card in order to speed the computation. The Caffe deep learning toolkit [109] was used in order to efficiently use the processing power of the Tesla graphics card for computation of convolutional neural network parameters. It takes approximately 10 hours to train the proposed neural network using the mentioned hardware. The testing was done on the DRiDB database [97], which is explained in more detail in Chapter 3. The database was split into two disjoint sets for training and testing purposes.

Table 7.2: Results of different exudate detection methods.

Method name	Sensitivity	PPV	F-Score
Walter [84]	0.69	0.48	0.57
Sánchez [95]	0.34	0.61	0.44
Harangi [85]	0.66	0.65	0.66
Harangi [93]	0.71	0.66	0.68
Amel [91]	0.41	0.09	0.15
Weighted ensemble based exudate detection method	0.75	0.77	0.76
Expert system based exudate detection method	0.78	0.78	0.78

To test the method the ground truth data available in the mentioned datasets was used. For each image, number of true positives (TP), false positives (FP) and false negatives (FN) is calculated. The procedure for calculating the number of true positives, false positives and false negatives is explained in performance evaluation section in Chapter 6.

Table 7.2 presents the results of the experimental validation after 3-fold cross-validation for the DRiDB database. The proposed method outperforms all algorithms used in the validation process. In Fig. 7.9 the results of the proposed method can be seen. Also, we can notice that the performance is better compared to the original exudate detection method presented in

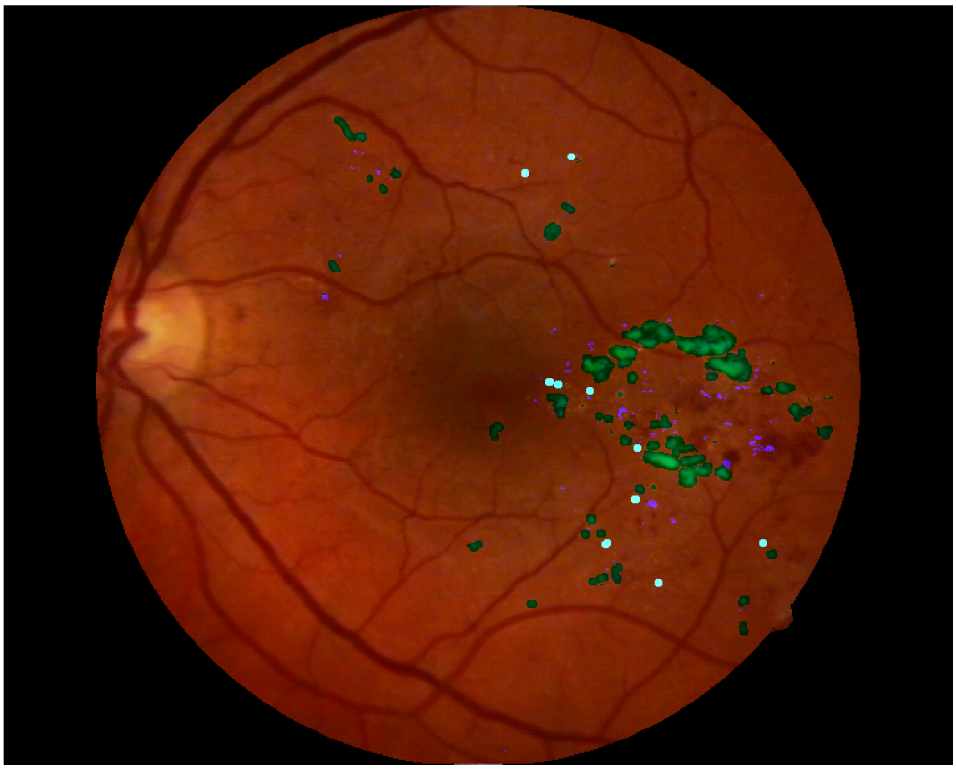

Fig. 7.9: Result obtained using the proposed deep learning based exudate detection method. Green: True positives, Blue: False positives, Cyan: False negatives

Chapter 6. From the example output image, it can be seen that the method misses small exudate groups but the main parts are detected properly.

Chapter 8

Conclusion

In the doctoral thesis developed methods for early automated detection of diabetic retinopathy were presented. The methods are based on advanced image processing and analysis algorithms, which use machine learning techniques in order to improve the overall performance.

During thesis work a database of 50 fundus images with labels was created. The database contains normal and pathological structures labeled by five opthatmological experts. Experts have labeled blood vessels, marked location of the optic disk and the macula region, segmented soft and hard exudates, small microaneurysms, small and large hemorrhages and neovascularizations. The database can be used for both method evaluation and algorithm development and is a very helpful tool for the diabetic research community. The database could be improved by gathering more images and accompanying labels. This would increase the usability of the database for algorithm development especially for deep learning approaches where large quantities of labeled data is required.

Developed optic disc detection method combines multiple simple optic detection algorithms to achieve good performance. Some of the methods, which are part of the ensemble are based on brightness thresholding, pyramidal decomposition of the input image, hough transform of main blood vessels, entropy filtering and are combined using a simple weighting scheme. The weights are found using the simulated annealing algorithm where number of missclassified images is the energy optimization function used. From our analysis the method has shown good performance over multiple test databases and more performance could be extracted if new optic disc detection methods were to be added in the pool of detectors. The method works well in both images without any pathologies and with images where severe pathologies related to diabetic retinopathy are present.

Exudates are an important visual symptom of diabetic retinopathy and early detection of exudates is of paramount importance in automated diabetic retinopathy screening systems. We developed an expert system based on ophthalmological knowledge which uses outputs of normal and pathological structure detectors in order to increase the overall exudate detection per-

formance. In order to detect exudate candidates, a deep convolutional neural network was trained on gathered database, which shows the algorithm development potential of our database. Overall performance of the exudate detection algorithm could be improved by incorporating even more ophthalmological knowledge in the segmentation procedure. Also, the performance could be improved by using newer and more advanced deep convolutional networks [110, 111]. In [112] authors presented a deep neural network, which can efficiently learn to make dense predictions for per-pixel tasks like semantic image segmentation. In our case, we have each exudate pixel segmented so applying such a network would be straightforward and should yield better results compared to our sliding window deep neural network approach.

The blood vessel detection method developed during thesis work is based on a model-based multi-scale approach. The method starts with an initial point and then estimates the vessel width and orientation within a local region at the processed point. After the vessel width and orientation are estimated, a small step is taken in the direction of the vessel direction. This procedure is repeated until the full vessel is traced out. The vessel width and orientation estimation is based on an model based optimization procedure. Using a two-dimensional model and a two-dimensional local region around the current point increases the accuracy and robustness of blood vessel orientation and width estimation procedure. The optimization procedure is not applied to raw pixel values of the image but to the blood vessel enhanced image where blood vessel enhancing is performed using a multi-scale Frangi vesselness filter. The method shows promising results and can be used as a part of a system for early detection of diabetic retinopathy, where location of blood vessels is important for locating other landmark points such as the optic disc or helping with pathology detection.

The focus of the thesis was on developing individual detection methods for optical disc localization, blood vessel segmentation and exudate segmentation. Due to increased capabilities of deep neural networks an area of improvement would be to use a holistic approach, where a single deep neural network could be applied directly on a particular fundus image and directly output the diabetic retinopathy severity level. In order to implement such a system a larger pool of images is required. But in this case only one label per image would be required so it would be much easier to gather such a dataset.

Bibliography

[1] Wild, S., Roglic, G., Green, A., Sicree, R., King, H., "Global prevalence of diabetes: estimates for the year 2000 and projections for 2030", Diabetes Care, Vol. 27, No. 5, 2004, str. 1047–1053.

[2] Lee, S. J., McCarty, C. A., Taylor, H. R., Keeffe, J. E., "Costs of mobile screening for diabetic retinopathy: a practical framework for rural populations", Aust J Rural Health, Vol. 9, No. 4, 2001, str. 186–192.

[3] McCarty, C. A., Lloyd-Smith, C. W., Lee, S. E., Livingston, P. M., Stanislavsky, Y. L., Taylor, H. R., "Use of eye care services by people with diabetes: the Melbourne Visual Impairment Project", Br J Ophthalmol, Vol. 82, No. 4, 1998, str. 410–414.

[4] Askew, D. A., Crossland, L., Ware, R. S., Begg, S., Cranstoun, P., Mitchell, P., Jackson, C. L., "Diabetic retinopathy screening and monitoring of early stage disease in general practice: design and methods", Contemp Clin Trials, Vol. 33, No. 5, 2012, str. 969–975.

[5] Looker, H. C., Nyangoma, S. O., Cromie, D., Olson, J. A., Leese, G. P., Black, M., Doig, J., Lee, N., Lindsay, R. S., McKnight, J. A., Morris, A. D., Philip, S., Sattar, N., Wild, S. H., Colhoun, H. M., "Diabetic retinopathy at diagnosis of type 2 diabetes in Scotland", Diabetologia, Vol. 55, No. 9, 2012, str. 2335–2342.

[6] Peto, T., Tadros, C., "Screening for diabetic retinopathy and diabetic macular edema in the United Kingdom", Curr. Diab. Rep., Vol. 12, No. 4, 2012, str. 338–345.

[7] Fraz, M. M., Remagnino, P., Hoppe, A., Uyyanonvara, B., Rudnicka, A. R., Owen, C. G., Barman, S. A., "Blood vessel segmentation methodologies in retinal images–a survey", Computer methods and programs in biomedicine, Vol. 108, No. 1, 2012, str. 407–433.

[8] Soares, J. V., Leandro, J. J., Cesar, R. M., Jelinek, H. F., Cree, M. J., "Retinal vessel segmentation using the 2-d gabor wavelet and supervised classification", IEEE Transactions on medical Imaging, Vol. 25, No. 9, 2006, str. 1214–1222.

[9] Kande, G. B., Subbaiah, P. V., Savithri, T. S., "Unsupervised fuzzy based vessel segmentation in pathological digital fundus images", Journal of medical systems, Vol. 34, No. 5, 2010, str. 849–858.

[10] Cinsdikici, M. G., Aydın, D., "Detection of blood vessels in ophthalmoscope images using mf/ant (matched filter/ant colony) algorithm", Computer methods and programs in biomedicine, Vol. 96, No. 2, 2009, str. 85–95.

[11] Sun, K., Chen, Z., Jiang, S., Wang, Y., "Morphological multiscale enhancement, fuzzy filter and watershed for vascular tree extraction in angiogram", Journal of medical systems, Vol. 35, No. 5, 2011, str. 811–824.

[12] Lam, B. S., Gao, Y., Liew, A. W.-C., "General retinal vessel segmentation using regularization-based multiconcavity modeling", IEEE Transactions on Medical Imaging, Vol. 29, No. 7, 2010, str. 1369–1381.

[13] Zhang, Y., Hsu, W., Lee, M. L., "Detection of retinal blood vessels based on nonlinear projections", Journal of Signal Processing Systems, Vol. 55, No. 1-3, 2009, str. 103.

[14] Roychowdhury, S., Koozekanani, D. D., Parhi, K. K., "Blood vessel segmentation of fundus images by major vessel extraction and subimage classification", IEEE journal of biomedical and health informatics, Vol. 19, No. 3, 2015, str. 1118–1128.

[15] Maji, D., Santara, A., Mitra, P., Sheet, D., "Ensemble of deep convolutional neural networks for learning to detect retinal vessels in fundus images", arXiv preprint arXiv:1603.04833, 2016.

[16] Jayaseelan, C. X., "Early detection of microaneurysms using retinal fundus images with removed blood vessel analysis", vol, Vol. 4, 2015, str. 1–10.

[17] Manimala, K., Gokulakrishnan, K., "Detection of microaneurysms in color fundus images", International Journal of Emerging Technology and Advanced Engineering, Vol. 4, No. 2, 2014, str. 30–7.

[18] Zhang, B., Wu, X., You, J., Li, Q., Karray, F., "Hierarchical detection of red lesions in retinal images by multiscale correlation filtering", in Medical Imaging 2009: Computer-Aided Diagnosis, Vol. 7260. International Society for Optics and Photonics, 2009, str. 72601L.

[19] Sánchez, C. I., Hornero, R., Mayo, A., García, M., "Mixture model-based clustering and logistic regression for automatic detection of microaneurysms in retinal images", in Medical Imaging 2009: Computer-Aided Diagnosis, Vol. 7260. International Society for Optics and Photonics, 2009, str. 72601M.

[20] Wu, B., Zhu, W., Shi, F., Zhu, S., Chen, X., "Automatic detection of microaneurysms in retinal fundus images", Computerized Medical Imaging and Graphics, Vol. 55, 2017, str. 106–112.

[21] Seoud, L., Hurtut, T., Chelbi, J., Cheriet, F., Langlois, J. P., "Red lesion detection using dynamic shape features for diabetic retinopathy screening", IEEE transactions on medical imaging, Vol. 35, No. 4, 2016, str. 1116–1126.

[22] Hassan, S. S. A., Bong, D. B., Premsenthil, M., "Detection of neovascularization in diabetic retinopathy", Journal of digital imaging, Vol. 25, No. 3, 2012, str. 437–444.

[23] Welfer, D., Scharcanski, J., Marinho, D. R., "A morphologic two-stage approach for automated optic disk detection in color eye fundus images", Pattern Recognition Letters, Vol. 34, No. 5, 2013, str. 476–485.

[24] Gao, W., Zuo, J., "Automated detection of hard exudates in fundus images using improved otsu thresholding and svm", International Journal of Computer Science & Engineering Survey, Vol. 7, No. 1, 2016, str. 1–11.

[25] van Grinsven, M. J., Theelen, T., Witkamp, L., van der Heijden, J., van de Ven, J. P., Hoyng, C. B., van Ginneken, B., Sánchez, C. I., "Automatic differentiation of color fundus images containing drusen or exudates using a contextual spatial pyramid approach", Biomedical optics express, Vol. 7, No. 3, 2016, str. 709–725.

[26] Niemeijer, M., van Ginneken, B., Russell, S. R., Suttorp-Schulten, M. S., Abràmoff, M. D., "Automated detection and differentiation of drusen, exudates, and cotton-wool spots in digital color fundus photographs for diabetic retinopathy diagnosis", Investigative ophthalmology & visual science, Vol. 48, No. 5, 2007, str. 2260–2267.

[27] van Grinsven, M. J., Lechanteur, Y. T., van de Ven, J. P., van Ginneken, B., Hoyng, C. B., Theelen, T., Sánchez, C. I., "Automatic drusen quantification and risk assessment of age-related macular degeneration on color fundus images", Investigative ophthalmology & visual science, Vol. 54, No. 4, 2013, str. 3019–3027.

[28] Niemeijer, M., Van Ginneken, B., Staal, J., Suttorp-Schulten, M. S., Abràmoff, M. D., "Automatic detection of red lesions in digital color fundus photographs", IEEE Transactions on medical imaging, Vol. 24, No. 5, 2005, str. 584–592.

[29] Giancardo, L., Meriaudeau, F., Karnowski, T. P., Li, Y., Tobin, K. W., Chaum, E., "Automatic retina exudates segmentation without a manually labelled training set", in Biomedical Imaging: From Nano to Macro, 2011 IEEE International Symposium on. IEEE, 2011, str. 1396–1400.

[30] Kirsch, R. A., "Computer determination of the constituent structure of biological images", Computers and biomedical research, Vol. 4, No. 3, 1971, str. 315–328.

[31] Niemeijer, M., Staal, J. J., Ginneken B. v., M., Loog, Abramoff, M. D. (2004) DRIVE: digital retinal images for vessel extraction, dostupno na: http://www.isi.uu.nl/Research/Databases/DRIVE

[32] Hoover, A., Kouznetsova, V., Goldbaum, M., "Locating blood vessels in retinal images by piecewise threshold probing of a matched filter response", Medical Imaging, IEEE Transactions on, Vol. 19, No. 3, 2000, str. 203-210.

[33] (2006) ARIA online, retinal image archive, dostupno na: http://www.eyecharity.com/doe/aria_online

[34] Kauppi, T., Kalesnykiene, V., Kamarainen, J. K., Lensu, L., Sorri, I., Raninen, A., Voutilainen, R., Uusitalo, H., Kälviäinen, H., Pietilä, J., "DIARETDB1 diabetic retinopathy database and evaluation protocol", Proc Medical Image Understanding and Analysis MIUA, Vol. 1, 2007, str. 3–7.

[35] (2004) MESSIDOR: Methods for evaluating segmentation and indexing techniques dedicated to retinal ophthalmology, dostupno na: http://messidor.crihan.fr/index-en.php

[36] Al-Diri, B., Hunter, A., Steel, D., Habib, M., Hudaib, T., Berry, S., "REVIEW-a reference data set for retinal vessel profiles", Engineering in Medicine and Biology Society,30th Annual International Conference of the IEEE, Vol. 2008, 2008, str. 2262-2265.

[37] Niemeijer, M., "Retinopathy online challenge: Automatic detection of microaneurysms in digital color fundus photographs", IEEE Trans. Med. Imaging, Vol. 29, 2009, str. 185–195.

[38] (2010) The VICAVR database, dostupno na: http://www.varpa.es/vicavr.html

[39] Poon, M., Hamarneh, G., Abugharbieh, R., "Live-vessel: Extending livewire for simultaneous extraction of optimal medial and boundary paths in vascular images", in Lecture Notes in Computer Science, Medical Image Computing and Computer-Assisted Intervention (MICCAI), 2007, str. 444-451.

[40] Sinthanayothin, C., Boyce, J. F., Cook, H. L., Williamson, T. H., "Automated localisation of the optic disc, fovea, and retinal blood vessels from digital colour fundus images", British Journal of Ophthalmology, Vol. 83, No. 8, 1999, str. 902–910.

[41] Gagnon, L., Lalonde, M., Beaulieu, M., Boucher, M.-C., "Procedure to detect anatomical structures in optical fundus images", in Medical Imaging 2001, 2001, str. 1218–1225.

[42] Li, H., Chutatape, O., "Automatic location of optic disk in retinal images", in Image Processing, 2001. Proceedings. 2001 International Conference on, Vol. 2, 2001, str. 837–840.

[43] Abdel-Ghafar, R. A., Morris, T., Ritchings, T., Wood, I., "Detection and characterisation of the optic disk in glaucoma and diabetic retinopathy", in Proceedings of Medical Image Understanding and Analysis, 2004.

[44] Ahmed, M. I., Amin, M. A., "High speed detection of optical disc in retinal fundus image", Signal, Image and Video Processing, Vol. 9, No. 1, 2015, str. 77–85.

[45] Hoover, A., Goldbaum, M., "Locating the optic nerve in a retinal image using the fuzzy convergence of the blood vessels", IEEE Transactions on Medical Imaging, Vol. 22, No. 8, 2003, str. 951–958.

[46] Ravishankar, S., Jain, A., Mittal, A., "Automated feature extraction for early detection of diabetic retinopathy in fundus images", in IEEE Conference on Computer Vision and Pattern Recognition, 2009. CVPR 2009., 2009, str. 210–217.

[47] Abdel-Razik, Y., Ghalwash, A. Z., Abdel-Rahman, G., "Optic disc detection from normalized digital fundus images by means of a vessels' direction matched filter", IEEE Transactions on Medical Imaging, Vol. 27, No. 1, 2008, str. 11–18.

[48] Osareh, A., Mirmehdi, M., Thomas, B., Markham, R., "Comparison of colour spaces for optic disc localisation in retinal images", in 16th International Conference on Pattern Recognition, 2002. Proceedings., Vol. 1, 2002, str. 743–746.

[49] ter Haar, F., "Automatic localization of the optic disc in digital colour images of the human retina", Doktorski rad, 2005.

[50] Sopharak, A., New, K. T., Moe, Y. A., Dailey, M. N., Uyyanonvara, B., "Automatic exudate detection with a naive bayes classifier", in Proceedings of the 2008 International Conference on Embedded Systems and Intelligent Technology, 2008, str. 139–142.

[51] Illingworth, J., Kittler, J., "A survey of the hough transform", Computer vision, graphics, and image processing, Vol. 44, No. 1, 1988, str. 87–116.

[52] Chaudhuri, S., Chatterjee, S., Katz, N., Nelson, M., Goldbaum, M., "Detection of blood vessels in retinal images using two-dimensional matched filters", IEEE transactions on medical imaging, Vol. 8, No. 3, 1989, str. 263–269.

[53] Frangi, A. F., Niessen, W. J., Vincken, K. L., Viergever, M. A., "Multiscale vessel enhancement filtering", in International Conference on Medical Image Computing and Computer-Assisted Intervention. Springer, 1998, str. 130–137.

[54] Walter, T., Klein, J.-C., "Segmentation of color fundus images of the human retina: Detection of the optic disc and the vascular tree using morphological techniques", in Medical Data Analysis. Springer, 2001, str. 282–287.

[55] Haralick, R. M., Shapiro, L. G., "Computer and robot vision, vol. i, 1992".

[56] Chen, J.-S., Huertas, A., Medioni, G., "Fast convolution with laplacian-of-gaussian masks", IEEE Transactions on Pattern Analysis and Machine Intelligence, No. 4, 1987, str. 584–590.

[57] Reza, A. M., "Realization of the contrast limited adaptive histogram equalization (clahe) for real-time image enhancement", Journal of VLSI signal processing systems for signal, image and video technology, Vol. 38, No. 1, 2004, str. 35–44.

[58] Otsu, N., "A threshold selection method from gray-level histograms", Automatica, Vol. 11, No. 285-296, 1975, str. 23–27.

[59] Granville, V., Krivánek, M., Rasson, J.-P., "Simulated annealing: A proof of convergence", IEEE transactions on pattern analysis and machine intelligence, Vol. 16, No. 6, 1994, str. 652–656.

[60] Al-Rawi, M., Qutaishat, M., Arrar, M., "An improved matched filter for blood vessel detection of digital retinal images", Computers in Biology and Medicine, Vol. 37, No. 2, 2007, str. 262–267.

[61] Zana, F., Klein, J.-C., "Segmentation of vessel-like patterns using mathematical morphology and curvature evaluation", IEEE transactions on image processing, Vol. 10, No. 7, 2001, str. 1010–1019.

[62] Mendonca, A. M., Campilho, A., "Segmentation of retinal blood vessels by combining the detection of centerlines and morphological reconstruction", IEEE transactions on medical imaging, Vol. 25, No. 9, 2006, str. 1200–1213.

[63] Mehrotra, A., Tripathi, S., Singh, K. K., Khandelwal, P., "Blood vessel extraction for retinal images using morphological operator and kcn clustering", in Advance Computing Conference (IACC), 2014 IEEE International. IEEE, 2014, str. 1142–1146.

[64] Imani, E., Javidi, M., Pourreza, H.-R., "Improvement of retinal blood vessel detection using morphological component analysis", Computer methods and programs in biomedicine, Vol. 118, No. 3, 2015, str. 263–279.

[65] Chutatape, O., Zheng, L., Krishnan, S., "Retinal blood vessel detection and tracking by matched gaussian and kalman filters", in Engineering in Medicine and Biology Society, 1998. Proceedings of the 20th Annual International Conference of the IEEE, Vol. 6. IEEE, 1998, str. 3144–3149.

[66] Staal, J., Abràmoff, M. D., Niemeijer, M., Viergever, M. A., van Ginneken, B., "Ridge-based vessel segmentation in color images of the retina", IEEE Transactions on Medical Imaging, Vol. 23, No. 4, 2004, str. 501–509.

[67] Wang, S., Yin, Y., Cao, G., Wei, B., Zheng, Y., Yang, G., "Hierarchical retinal blood vessel segmentation based on feature and ensemble learning", Neurocomputing, Vol. 149, 2015, str. 708–717.

[68] Marín, D., Aquino, A., Gegúndez-Arias, M. E., Bravo, J. M., "A new supervised method for blood vessel segmentation in retinal images by using gray-level and moment invariants-based features", IEEE transactions on medical imaging, Vol. 30, No. 1, 2011, str. 146–158.

[69] Vermeer, K. A., Vos, F. M., Lemij, H., Vossepoel, A. M., "A model based method for retinal blood vessel detection", Computers in Biology and Medicine, Vol. 34, No. 3, 2004, str. 209–219.

[70] Zhu, T., "Fourier cross-sectional profile for vessel detection on retinal images", Computerized Medical Imaging and Graphics, Vol. 34, No. 3, 2010, str. 203–212.

[71] Al-Diri, B., Hunter, A., Steel, D., "An active contour model for segmenting and measuring retinal vessels", IEEE Transactions on Medical imaging, Vol. 28, No. 9, 2009, str. 1488–1497.

[72] Cree, M., Cornforth, D., Jelinek, H., "Vessel segmentation and tracking using a two-dimensional model", IVC New Zealand, 2005, str. 345–350.

[73] Gao, X. W., Bharath, A., Stanton, A., Hughes, A., Chapman, N., Thom, S., "Quantification and characterisation of arteries in retinal images", Computer methods and programs in biomedicine, Vol. 63, No. 2, 2000, str. 133–146.

[74] Gao, X., Bharath, A. A., Hughes, A. J., Stanton, A., Chapman, N., Thom, S., "Toward retinal vessel parameterization", in Medical Imaging 1997. International Society for Optics and Photonics, 1997, str. 734–744.

[75] Brinchmann-Hansen, O., Heier, H., "Theoretical relations between light streak characteristics and optical properties of retinal vessels", Acta Ophthalmologica, Vol. 64, No. S179, 1986, str. 33–37.

[76] Li, H., Hsu, W., Lee, M. L., Wong, T. Y., "Automatic grading of retinal vessel caliber", IEEE Transactions on Biomedical Engineering, Vol. 52, No. 7, 2005, str. 1352–1355.

[77] Florack, L. M., ter Haar Romeny, B. M., Koenderink, J. J., Viergever, M. A., "Scale and the differential structure of images", Image and Vision Computing, Vol. 10, No. 6, 1992, str. 376–388.

[78] Koenderink, J. J., "The structure of images", Biological cybernetics, Vol. 50, No. 5, 1984, str. 363–370.

[79] Lindeberg, T., "Edge detection and ridge detection with automatic scale selection", in Computer Vision and Pattern Recognition, 1996. Proceedings CVPR'96, 1996 IEEE Computer Society Conference on. IEEE, 1996, str. 465–470.

[80] Marquardt, D. W., "An algorithm for least-squares estimation of nonlinear parameters", Journal of the Society for Industrial & Applied Mathematics, Vol. 11, No. 2, 1963, str. 431–441.

[81] Youssif, A. A., Ghalwash, A. Z., Ghoneim, A. S., "Comparative study of contrast enhancement and illumination equalization methods for retinal vasculature segmentation", in Proceedings of the Third Cairo International Biomedical Engineering Conference (CIBEC'06), 2006, str. 1–5.

[82] Xiao, Z., Li, F., Geng, L., Zhang, F., Wu, J., Zhang, X., Su, L., Shan, C., Yang, Z., Sun, Y. *et al.*, "Hard exudates detection method based on background-estimation", in International Conference on Image and Graphics. Springer, 2015, str. 361–372.

[83] Goatman, K. A., Whitwam, A. D., Manivannan, A., Olson, J. A., Sharp, P. F., "Colour normalisation of retinal images", in Proceedings of Medical Image Understanding and Analysis, 2003, str. 49–52.

[84] Walter, T., Klein, J.-C., Massin, P., Erginay, A., "A contribution of image processing to the diagnosis of diabetic retinopathy-detection of exudates in color fundus images of the human retina", Medical Imaging, IEEE Transactions on, Vol. 21, No. 10, 2002, str. 1236–1243.

[85] Harangi, B., Antal, B., Hajdu, A., "Automatic exudate detection with improved naïve-bayes classifier", in Computer-Based Medical Systems (CBMS), 2012 25th International Symposium on. IEEE, 2012, str. 1–4.

[86] Annunziata, R., Garzelli, A., Ballerini, L., Mecocci, A., Trucco, E., "Leveraging multiscale hessian-based enhancement with a novel exudate inpainting technique for retinal vessel segmentation", Journal of biomedical and health informatics, 2015.

[87] Sánchez, C. I., García, M., Mayo, A., López, M. I., Hornero, R., "Retinal image analysis based on mixture models to detect hard exudates", Medical Image Analysis, Vol. 13, No. 4, 2009, str. 650–658.

[88] Sopharak, A., Uyyanonvara, B., Barman, S., "Automatic exudate detection from non-dilated diabetic retinopathy retinal images using fuzzy c-means clustering", Sensors, Vol. 9, No. 3, 2009, str. 2148–2161.

[89] Rokade, P. M., Manza, R. R., "Automatic detection of hard exudates in retinal images using haar wavelet transform", International Journal of Application or Innovation in Engineering and Management, Vol. 4, No. 5, 2015, str. 402–410.

[90] Osareh, A., Mirmehdi, M., Thomas, B., Markham, R., "Automatic recognition of exudative maculopathy using fuzzy c-means clustering and neural networks", in Proc. Medical Image Understanding Analysis Conf, Vol. 3, 2001, str. 49–52.

[91] Amel, F., Mohammed, M., Abdelhafid, B., "Improvement of the hard exudates detection method used for computer-aided diagnosis of diabetic retinopathy.", International Journal of Image, Graphics & Signal Processing, Vol. 4, No. 4, 2012.

[92] Saánchez, C. I., Niemeijer, M., Suttorp Schulten, M. S., Abraámoff, M., van Ginneken, B., "Improving hard exudate detection in retinal images through a combination of local and contextual information", in Biomedical Imaging: From Nano to Macro, 2010 IEEE International Symposium on. IEEE, 2010, str. 5–8.

[93] Harangi, B., Lazar, I., Hajdu, A., "Automatic exudate detection using active contour model and regionwise classification", in Engineering in Medicine and Biology Society (EMBC), 2012 Annual International Conference of the IEEE. IEEE, 2012, str. 5951–5954.

[94] Sánchez, C. I., Niemeijer, M., Išgum, I., Dumitrescu, A., Suttorp-Schulten, M. S., Abràmoff, M. D., van Ginneken, B., "Contextual computer-aided detection: Improving bright lesion detection in retinal images and coronary calcification identification in ct scans", Medical image analysis, Vol. 16, No. 1, 2012, str. 50–62.

[95] Sánchez, C. I., Hornero, R., López, M. I., Aboy, M., Poza, J., Abasolo, D., "A novel automatic image processing algorithm for detection of hard exudates based on retinal image analysis", Medical Engineering & Physics, Vol. 30, No. 3, 2008, str. 350–357.

[96] Garcia, M., Sánchez, C. I., Poza, J., López, M. I., Hornero, R., "Detection of hard exudates in retinal images using a radial basis function classifier", Annals of biomedical engineering, Vol. 37, No. 7, 2009, str. 1448–1463.

[97] Prentasic, P., Loncaric, S., Vatavuk, Z., Bencic, G., Subasic, M., Petkovic, T., Dujmovic, L., Malenica-Ravlic, M., Budimlija, N., Tadic, R., "Diabetic retinopathy image database (dridb): a new database for diabetic retinopathy screening programs research", in 8th International Symposium on Image and Signal Processing and Analysis (ISPA), 2013, str. 711–716.

[98] Abdou, I. E., Pratt, W. K., "Quantitative design and evaluation of enhancement/thresholding edge detectors", Proceedings of the IEEE, Vol. 67, No. 5, 1979, str. 753–763.

[99] Woolson, R., "Wilcoxon signed-rank test", Wiley encyclopedia of clinical trials, 2008.

[100] Zhang, X., Thibault, G., Decenciere, E., Marcotegui, B., Laÿ, B., Danno, R., Cazuguel, G., Quellec, G., Lamard, M., Massin, P. *et al.*, "Exudate detection in color retinal images for mass screening of diabetic retinopathy", Medical image analysis, Vol. 18, No. 7, 2014, str. 1026–1043.

[101] Tobin, K. W., Chaum, E., Govindasamy, V. P., Karnowski, T. P., "Detection of anatomic structures in human retinal imagery", Medical Imaging, IEEE Transactions on, Vol. 26, No. 12, 2007, str. 1729–1739.

[102] Masci, J., Giusti, A., Cireşan, D., Fricout, G., Schmidhuber, J., "A fast learning algorithm for image segmentation with max-pooling convolutional networks", arXiv preprint arXiv:1302.1690, 2013.

[103] Rudin, L. I., Osher, S., Fatemi, E., "Nonlinear total variation based noise removal algorithms", Physica D: Nonlinear Phenomena, Vol. 60, No. 1, 1992, str. 259–268.

[104] Goldstein, T., Osher, S., "The split bregman method for l1-regularized problems", SIAM Journal on Imaging Sciences, Vol. 2, No. 2, 2009, str. 323–343.

[105] Getreuer, P., "Rudin-osher-fatemi total variation denoising using split bregman", Image Processing On Line, Vol. 10, 2012.

[106] Ciresan, D., Giusti, A., Gambardella, L. M., Schmidhuber, J., "Deep neural networks segment neuronal membranes in electron microscopy images", in Advances in neural information processing systems, 2012, str. 2843–2851.

[107] Ciresan, D., Meier, U., Schmidhuber, J., "Multi-column deep neural networks for image classification", in Computer Vision and Pattern Recognition (CVPR), 2012 IEEE Conference on. IEEE, 2012, str. 3642–3649.

[108] Winder, R. J., Morrow, P. J., McRitchie, I. N., Bailie, J., Hart, P. M., "Algorithms for digital image processing in diabetic retinopathy", Computerized Medical Imaging and Graphics, Vol. 33, No. 8, 2009, str. 608–622.

[109] Jia, Y., Shelhamer, E., Donahue, J., Karayev, S., Long, J., Girshick, R., Guadarrama, S., Darrell, T., "Caffe: Convolutional architecture for fast feature embedding", arXiv preprint arXiv:1408.5093, 2014.

[110] He, K., Zhang, X., Ren, S., Sun, J., "Deep residual learning for image recognition", in Proceedings of the IEEE conference on computer vision and pattern recognition, 2016, str. 770–778.

[111] Larsson, G., Maire, M., Shakhnarovich, G., "Fractalnet: Ultra-deep neural networks without residuals", arXiv preprint arXiv:1605.07648, 2016.

[112] Long, J., Shelhamer, E., Darrell, T., "Fully convolutional networks for semantic segmentation", in Proceedings of the IEEE conference on computer vision and pattern recognition, 2015, str. 3431–3440.

Životopis

Pavle Prentašić rođen je 5. lipnja 1989. godine u Sremskoj Mitrovici. Završio je opću gimnaziju Fran Galović u Koprivnici 2007. godine kada upisuje Fakultet elektrotehnike i računarstva, Sveučilište u Zagrebu (FER). Pavle je dobio titulu sveučilišnog prvostupnika inženjera računarstva 2010. godine pod mentorstvom profesora Svena Lončarića. Pavle je dobio titulu magistra inženjera računarstva 2012. godine pod mentorsvom profesora Svena Lončarića. Iste godine Pavle je upisao doktorski studij računarstva na Fakultetu elektrotehnike i računarstva. Autor je dva znanstvena rada u časopisama, autor ili koautor 9 znanstvenih radova u zbornicima skupova s međunarodnom recenzijom te je vlasnik jednog patenta. Član je IEEE-a.

Popis objavljenih djela

Rad u časopisima

1. Prentašić, P., Heisler, M., Mammo, Z., Lee, S., Merkur, A., Navajas, E., Faisal Beg, M., Šarunić, M., Lončarić, S., Segmentation of the foveal microvasculature using deep learning networks, Journal of biomedical optics, Vol. 21, No. 7, 2016, 075008-1-075008-7
2. Prentašić, P., Lončarić, S., Detection of exudates in fundus photographs using deep neural networks and anatomical landmark detection fusion, Computer methods and programs in biomedicine, Vol. 137, 2016, 281-292.

Biography

Pavle Prentašić was born on June 5th 1989 in Sremska Mitrovica. He finished his high school education at Fran Galović high school from Koprivnica in 2007. He obtained his bachelors degree in computing from University of Zagreb, Faculty of Electrical Engineering and Computing in 2010 under supervision of professor Sven Lončarić. He obtained his masters of engineering in computing science degree with highest honor in 2012 from University of Zagreb, Faculty of Electrical Engineering and Computing under supervision of professor Sven Lončarić. Pavle started his doctoral studies in 2012. He is author of two journal papers, author or co-author of nine conference papers and owns one patent. He is a member of IEEE.